Long-Term Embrittlement of Cast Duplex Stainless Steels in LWR Systems

Semiannual Report
October 1989–March 1990

Prepared by O. K. Chopra, L. Y. Bush

Argonne National Laboratory

Long-Term Embrittlement of Cast Duplex Stainless Steels in LWR Systems

Semiannual Report
October 1989–March 1990

Prepared by
O. K. Chopra, L. Y. Bush

Argonne National Laboratory
9700 South Cass Avenue
Argonne, IL 60439

Previous Documents in Series

Long–Term Embrittlement of Cast Duplex Stainless Steels in LWR Systems: Annual Report, October 1982–September 1983, NUREG/CR–3857, ANL–84–44 (August 1984).

Long–Term Embrittlement of Cast Duplex Stainless Steels in LWR Systems: Annual Report, October 1983–September 1984, NUREG/CR–4204, ANL–85–20 (March 1985).

Long–Term Embrittlement of Cast Duplex Stainless Steels in LWR Systems: Annual Report, October 1984–September 1985, NUREG/CR–4503, ANL–86–3 (January 1986).

Long–Term Embrittlement of Cast Duplex Stainless Steels in LWR Systems: Semiannual Report, October 1985–March 1986, NUREG/CR–4744 Vol. 1, No. 1, ANL–86–54 (January 1987).

Long–Term Embrittlement of Cast Duplex Stainless Steels in LWR Systems: Semiannual Report, April–September 1986, NUREG/CR–4744 Vol. 1, No. 2, ANL–87–16 (March 1987).

Long–Term Embrittlement of Cast Duplex Stainless Steels in LWR Systems: Semiannual Report, October 1986–March 1987, NUREG/CR–4744, Vol. 2, No. 1, ANL–87–45 (July 1987).

Long–Term Embrittlement of Cast Duplex Stainless Steels in LWR Systems: Semiannual Report, April–September 1987, NUREG/CR–4744, Vol. 2, No. 2, ANL–89/6 (August 1989).

Long–Term Embrittlement of Cast Duplex Stainless Steels in LWR Systems: Semiannual Report, October 1987–March 1988, NUREG/CR–4744, Vol. 3, No. 1, ANL–89/22 (February 1990).

Long–Term Embrittlement of Cast Duplex Stainless Steels in LWR Systems: Semiannual Report, April–September 1988, NUREG/CR–4744, Vol. 3, No. 2, ANL–90/5 (August 1990).

Long–Term Embrittlement of Cast Duplex Stainless Steels in LWR Systems: Semiannual Report, October 1988–March 1989, NUREG/CR–4744, Vol. 4, No. 1, ANL–90/44 (May 1991).

Long–Term Embrittlement of Cast Duplex Stainless Steels in LWR Systems: Semiannual Report, April–September 1989, NUREG/CR–4744, Vol. 4, No. 2, ANL–90/49 (June 1991).

Long–Term Embrittlement of Cast Duplex Stainless Steels in LWR Systems

by

O. K. Chopra and L. Y. Bush

Abstract

This progress report summarizes work performed by Argonne National Laboratory on long–term thermal embrittlement of cast duplex stainless steels in LWR systems during the six months from October 1989 to March 1990. The results from Charpy–impact tests and microhardness measurements of the ferrite phase for several heats of cast stainless steel aged up to 30,000 h at 290–400°C are analyzed to establish the kinetics of thermal embrittlement. Correlations are presented for predicting the extent and kinetics of thermal embrittlement of cast stainless steels from material information that can be determined from the certified material test record. The extent of embrittlement is characterized by the room–temperature "normalized" Charpy–impact energy. Based on the information available, two methods are presented for estimating the extent of embrittlement at "saturation," i.e., the minimum impact energy that would be achieved for the material after long–term aging. The first method utilizes only the chemical composition of the steel. The second method is used when metallographic information on the ferrite morphology, i.e., measured values of ferrite content and mean ferrite spacing of the steel, is also available. The change in Charpy–impact energy as a function of time and temperature of reactor service is then estimated from the extent of embrittlement at saturation and from the correlations describing the kinetics of embrittlement, which is expressed in terms of the chemical composition and aging behavior of the steel at 400°C.

Contents

List of Figures

List of Tables

Executive Summary

Cast stainless steels used in pump casings, valve bodies, piping, and other components in coolant systems of light water nuclear reactors (LWRs) suffer a loss in toughness after many years of service at temperatures in the range of 290–320°C (≈554–608°F). A program is being conducted to investigate the low-temperature thermal embrittlement of cast duplex stainless steels under LWR operating conditions and to evaluate possible remedies for the thermal embrittlement problem in existing and future plants. The scope of the investigation includes the following goals: (1) characterize and correlate the microstructure of in-service reactor components and laboratory–aged material with loss of fracture toughness to establish the mechanism of aging and validate the simulation of in–reactor degradation by accelerated aging, (2) establish the effects of key compositional and metallurgical variables on the kinetics and extent of thermal embrittlement, and (3) develop the methodology and correlations necessary for predicting the toughness loss suffered by cast stainless steel components during the normal and extended life of LWRs.

Microstructural and mechanical–property data are being obtained on 25 experimental heats (static-cast keel blocks and slabs) and 6 commercial heats (centrifugally cast pipes, a static-cast pump impeller, and a static-cast pump casing ring), as well as on reactor-aged material of CF-3, CF-8, and CF-8M grades of cast stainless steel. The ferrite content of the cast materials ranges from 3 to 30%. Ferrite morphology for the castings containing >5% ferrite is either lacy or acicular.

Charpy-impact, tensile, and J-R curve tests have been conducted on several experimental and commercial heats of cast stainless steel that were aged up to 30,000 h at temperatures of 290–400°C (554–752°F). Results indicate that thermal aging at these temperatures increases the tensile strength and decreases the impact energy and fracture toughness of the steels. The Charpy transition curve shifts to higher temperatures. Different heats exhibit different degrees of thermal embrittlement. In general, the low-carbon CF-3 steels are the most resistant, and the molybdenum-bearing, high-carbon CF-8M steels are the least resistant to thermal embrittlement. Embrittlement of cast stainless steels results in brittle fracture associated with either cleavage of the ferrite or separation of the ferrite/austenite phase boundary. A predominantly brittle failure occurs when either the ferrite phase is continuous, e.g., in cast material with a high ferrite content, or the ferrite/austenite phase boundary provides an easy path for crack propagation, e.g., in high-carbon grades of cast steels with phase-boundary carbides. Consequently, the amount, size, and distribution of the ferrite phase in the duplex structure and the presence of phase-boundary carbides are important parameters in controlling the degree or extent of thermal embrittlement.

Thermal aging of cast stainless steels at temperatures <500°C (<932°F) leads to precipitation of additional phases in the ferrite matrix, e.g., formation of a chromium-rich α' phase by spinodal decomposition; nucleation and growth of α'; precipitation of a nickel– and silicon–rich G phase, $M_{23}C_6$ carbide, and γ_2 (austenite); and additional precipitation and/or growth of existing carbides at the ferrite/austenite phase boundaries. The additional phases provide the strengthening mechanisms that increase strain hardening and local tensile stress. Consequently, the critical stress level for brittle fracture is achieved at higher tem-

peratures. The effects of material variables on the thermal embrittlement of cast stainless steels have been evaluated.

This report presents an analysis of the data from Charpy-impact tests and ferrite hardness measurements for several heats of cast stainless steel aged up to 30,000 h at 290–400°C (554–752°F), to establish the kinetics of thermal embrittlement. The results indicate that the aging behavior at 400°C varies significantly for the various heats of cast stainless steel. The production heat treatment and possibly the casting process influence the aging behavior at 400°C and therefore the kinetics of embrittlement. The activation energy for thermal embrittlement determined from measurements of ferrite hardness agree very well with that obtained from Charpy-impact data. Studies on the re-embrittlement of recovery-annealed materials indicate that precipitation of G phase has little or no effect on the kinetics of thermal embrittlement. Material and aging parameters that influence the kinetics of embrittlement have been discussed. A correlation is presented for estimating the activation energy of thermal embrittlement from the chemical composition and aging behavior of the steel at 400°C.

Correlations are also presented for estimating the extent of thermal embrittlement of cast stainless steels from material information that can be determined from the certified material test record. The extent of embrittlement is characterized by the room-temperature "normalized" Charpy-impact energy. Correlations for the extent of embrittlement at "saturation," i.e., the minimum impact energy that can be achieved for the material after long-term aging, is given in terms of a material parameter that consists of the chemical composition and ferrite morphology. Different correlations are used for estimating the saturation impact energy of CF-3 or CF-8 steels and CF-8M steels. A common expression between material parameter and saturation impact energy is used when metallographic information, i.e., the measured values of ferrite content and mean ferrite spacing, is known. The change in Charpy-impact energy as a function of time and temperature of reactor service is then estimated from the extent of embrittlement at saturation and from the correlation describing the kinetics of embrittlement. Examples for estimating impact strength of cast stainless steel components during reactor service are described.

2

1   Introduction

Cast duplex stainless steels used in LWR systems for primary pressure-boundary components such as valve bodies, pump casings, and primary coolant piping are susceptible to thermal embrittlement at reactor operating temperatures, i.e., 290–320°C (≈554–608°F). Aging of cast stainless steels at these temperatures causes an increase in hardness and tensile strength and a decrease in ductility, impact strength, and fracture toughness of the material. Most studies on thermal embrittlement of cast stainless steels involve simulation of end-of-life reactor conditions by accelerated aging at higher temperatures, viz., 400°C (752°F), because the time period for operation of power plant (≈40 y) is far longer than can generally be considered for laboratory studies. Thus, estimates of the loss of fracture toughness suffered by cast stainless steel components are based on an Arrhenius extrapolation of the high-temperature data to reactor operating conditions.

A program is being conducted to investigate the significance of low-temperature thermal embrittlement of cast duplex stainless steels under light-water reactor (LWR) operating conditions and to evaluate possible remedies to the thermal embrittlement problem in existing and future plants. The scope of the program includes the following goals: (1) characterize and correlate the microstructure of in-service reactor components and laboratory-aged material with loss of fracture toughness to establish the mechanism of aging and validate the simulation of in-reactor degradation by accelerated aging, (2) establish the effects of key compositional and metallurgical variables on the kinetics and extent of thermal embrittlement, and (3) develop the methodology and correlations necessary for predicting the toughness loss suffered by cast stainless steel components during the normal and extended life of LWRs.

Microstructural and mechanical-property data are being obtained on 25 experimental heats (static-cast keel blocks) and 6 commercial heats (centrifugally cast pipes, a static-cast pump impeller, and a static-cast pump casing ring), as well as on reactor-aged material of grades CF–3, CF–8, and CF–8M cast stainless steels. Six of the experimental heats are in the form of 76-mm-thick slabs. Specimen blanks for Charpy-impact, tensile, and J-R curve tests have been aged at 290, 320, 350, 400, and 450°C (554, 608, 662, 752, and 842°F) for times up to 60,000 h. The reactor-aged material is from the recirculating-pump cover plate assembly of the KRB reactor, which was in service in Gundremmingen, West Germany, for ≈8 y at a service temperature of 284°C (543°F). Fractured impact-test bars from five heats of aged cast stainless steel were obtained from the Georg Fischer Co. (GF), Switzerland, for microstructural characterization. The materials are from a previous study of long-term aging behavior of cast stainless steel.[1] The data on chemical composition, ferrite content, hardness, ferrite morphology, and grain structure of the various heats have been reported earlier.[2-6] Chemical composition, hardness, and ferrite content and distribution of the cast materials are given in Table 1. The results of microstructural characterization and mechanical-property data from Charpy-impact, tensile, and J-R curve tests on 16 heats of cast stainless steel aged up to 30,000 h at temperatures between 290–450°C have also been presented earlier.[7-20]

Work at Argonne National Laboratory (ANL) and elsewhere[1,21-27] has shown that thermal embrittlement of cast stainless steel components will occur during the reactor lifetime of 40 y. Thermal aging at reactor temperatures increases the tensile stress and decreases

Table 1. *Product form, chemical composition, hardness, and ferrite morphology of various heats of cast stainless steels*

Heat	Grade	Chemical Composition (wt.%)									Hardness R_B	Ferrite[a] (%)		Ferrite Spacing (μm)
		Mn	Si	P	S	Mo	Cr	Ni	N	C		Calc.	Meas.	
							Keel Blocks[b]							
50	CF-3	0.60	1.10	0.016	0.007	0.33	17.89	9.14	0.079	0.034	80.1	3.0	4.4	194
49	CF-3	0.60	0.95	0.010	0.007	0.32	19.41	10.69	0.065	0.010	76.6	4.4	7.2	185
48	CF-3	0.60	1.08	0.009	0.006	0.30	19.55	10.46	0.072	0.011	78.1	5.1	8.7	127
47	CF-3	0.60	1.06	0.007	0.006	0.59	19.81	10.63	0.028	0.018	79.7	8.4	16.3	68
52	CF-3	0.57	0.92	0.012	0.005	0.35	19.49	9.40	0.052	0.009	81.6	10.3	13.5	69
51	CF-3	0.63	0.86	0.014	0.005	0.32	20.13	9.06	0.058	0.010	83.8	14.3	18.0	52
58	CF-8	0.62	1.12	0.010	0.005	0.33	19.53	10.89	0.040	0.056	77.1	3.2	2.9	303
54	CF-8	0.55	1.03	0.011	0.005	0.35	19.31	9.17	0.084	0.063	83.3	4.1	1.8	317
57	CF-8	0.62	1.08	0.009	0.004	0.34	18.68	9.27	0.047	0.056	80.2	4.4	4.0	138
53	CF-8	0.64	1.16	0.012	0.009	0.39	19.53	9.23	0.049	0.065	83.1	6.3	8.7	92
56	CF-8	0.57	1.05	0.007	0.007	0.34	19.65	9.28	0.030	0.066	82.5	7.3	10.1	84
59	CF-8	0.60	1.08	0.008	0.007	0.32	20.33	9.34	0.045	0.062	83.2	8.8	3.5	75
61	CF-8	0.65	1.01	0.007	0.007	0.32	20.65	8.86	0.080	0.054	85.3	10.0	13.1	82
60	CF-8	0.67	0.95	0.008	0.006	0.31	21.05	8.34	0.058	0.064	86.7	15.4	21.1	63
62	CF-8M	0.72	0.56	0.007	0.005	2.57	18.29	12.39	0.030	0.063	78.1	2.8	4.5	140
63	CF-8M	0.61	0.58	0.007	0.006	2.57	19.37	11.85	0.031	0.055	81.6	6.4	10.4	81
66	CF-8M	0.60	0.49	0.012	0.007	2.39	19.45	9.28	0.029	0.047	85.3	19.6	19.8	41
65	CF-8M	0.50	0.48	0.012	0.007	2.57	20.78	9.63	0.064	0.049	89.0	20.9	23.4	43
64	CF-8M	0.60	0.63	0.006	0.005	2.46	20.76	9.40	0.038	0.038	89.7	29.0	28.4	41
							76-mm Slabs[c]							
69	CF-3	0.63	1.13	0.015	0.005	0.34	20.18	8.59	0.028	0.023	83.7	21.0	23.6	35
73	CF-8	0.72	1.09	0.028	0.016	0.25	19.43	8.54	0.053	0.070	78.8	7.0	7.7	253
68	CF-8	0.64	1.07	0.021	0.014	0.31	20.64	8.08	0.062	0.063	84.6	14.9	23.4	87
70	CF-8M	0.55	0.72	0.021	0.016	2.30	19.17	9.01	0.049	0.066	86.5	14.2	18.9	96
74	CF-8M	0.54	0.73	0.022	0.016	2.51	19.11	9.03	0.048	0.064	85.8	15.5	18.4	90
75	CF-8M	0.53	0.67	0.022	0.012	2.58	20.86	9.12	0.052	0.065	89.5	24.5	27.8	69
							Reactor Components[d]							
P3	CF-3	1.06	0.88	0.017	0.014	0.01	18.89	8.45	0.168	0.021	82.2	2.8	1.9	–
P2	CF-3	0.74	0.94	0.019	0.006	0.16	20.20	9.38	0.040	0.019	83.8	12.5	15.6	69
1	CF-3	0.47	0.83	0.030	0.011	0.45	20.20	8.70	0.032	0.019	81.0	20.4	17.1	65
C1	CF-8	1.22	1.18	0.033	0.008	0.65	19.00	9.37	0.040	0.039	79.5	7.8	2.2	–
P1	CF-8	0.59	1.12	0.026	0.013	0.04	20.49	8.10	0.056	0.036	84.9	17.7	24.1	90
P4	CF-8M	1.07	1.02	0.019	0.015	2.05	19.64	10.00	0.151	0.040	83.1	5.9	10.0	182
205	CF-8M	0.93	0.63	0.019	–	3.37	17.88	8.80	–	0.040	–	21.0	15.9	79
758	CF-8M	0.91	0.62	0.018	–	3.36	17.91	8.70	–	0.030	–	24.2	19.2	62
							Reactor-Aged[e]							
KRB	CF-8	0.31	1.17	–	–	0.17	21.99	8.03	0.038	0.062	–	27.7	34.0	–

Table 1. (Contd.)

Heat	Grade	Chemical Composition (wt.%)									Hardness R_B	Ferrite[a] (%)		Ferrite Spacing (μm)
		Mn	Si	P	S	Mo	Cr	Ni	N	C		Calc.	Meas.	
					Laboratory-Aged[f]									
280	CF-3	0.50	1.37	0.015	0.006	0.25	21.60	8.00	0.038	0.028	–	36.3	40.0	186
278	CF-8	0.28	1.00	0.008	0.019	0.13	20.20	8.27	0.030	0.038	–	18.5	15.0	174
292	CF-8	0.34	1.57	0.018	0.016	0.13	21.60	7.52	0.039	0.090	–	23.9	28.0	–
286	CF-8M	0.40	1.33	0.044	0.015	2.44	20.20	9.13	0.062	0.072	–	18.9	22.0	201

[a] Calculated from the composition with Hull's equivalent factor.
Measured by ferrite scope AUTO Test FE, Probe Type FSP-1.
[b] Static Cast Keel Blocks: Foundry ESCO; Size 180 x 120 x 90–30 mm.
[c] Static Cast Slabs: Foundry ESCO; Size 610 x 610 x 76 mm.
[d] Centrifugally Cast Pipes:
    P3 Foundry SANDUSKY; Size 580 mm O.D.,76 mm wall.
    P2 Foundry FAM, France; Size 930 mm O.D., 73 mm wall.
    P1 Foundry ESCO; Size 890 mm O.D., 63 mm wall.
    P4 Foundry SANDUSKY; Size 580 mm O.D., 32 mm wall.
    205 Size 305 mm O.D., 25 mm wall.
  Static Cast:
    Elbow 758: Size 305 mm O.D., 30 mm wall.
    Pump Impeller I: Foundry ESCO; Size 660 mm diameter.
    Pump Casing C1: Foundry ESCO; Size 600 mm O.D., 57 mm wall.
[e] KRB Reactor Pump Cover Plate: Foundry GF; Size 890 mm diameter.
[f] Aged Material from Georg Fischer Co., Switzerland.

the impact energy and fracture toughness of the steels. The Charpy transition curve shifts to higher temperatures. Different heats exhibit different degrees of thermal embrittlement. For cast stainless steel of all grades, the extent of embrittlement increases with an increase in ferrite content. The low-carbon (C) CF-3 steels are the most resistant, and the molybdenum (Mo)-bearing, high-C CF-8M steels are the least resistant to thermal embrittlement. The flow stress of fully aged CF-3 steels increases by ≈10% and of CF-8 and CF-8M steels by ≈20%. The fracture toughness J_{IC} and average tearing modulus for heats that are sensitive to thermal aging (e.g., CF-8M steels) are as low as ≈90 kJ/m^2 and ≈60, respectively. Correlations have been developed for estimating the increase in flow stress of the steels from data for the kinetics of thermal embrittlement.[15]

The mechanisms of thermal embrittlement of cast duplex stainless steel have been discussed.[12] Embrittlement of cast stainless steels results in a brittle fracture associated with either cleavage of the ferrite or separation of the ferrite/austenite phase boundary. The degree of thermal embrittlement is controlled by the amount of brittle fracture. Cast stainless steels with poor impact strength exhibit >80% brittle fracture. In some cast steels, a fraction of the material may fail in a brittle fashion but the surrounding austenite provides ductility and toughness. Such steels have adequate impact strength even after long-term aging. Predominantly brittle failure occurs when either the ferrite phase is continuous, e.g., in cast material with a high ferrite content, or the ferrite/austenite phase boundary provides an easy path for crack propagation, e.g., in high-C grades of cast steels with phase-boundary carbides. Consequently, the amount, size, and distribution of the ferrite phase in the duplex structure and the presence of phase-boundary carbides are important parameters in controlling the degree or extent of thermal embrittlement.

Thermal aging of cast stainless steels at <500°C (<932°F) leads to precipitation of additional phases in the ferrite matrix, e.g., formation of a chromium (Cr)-rich α' phase by spinodal decomposition; nucleation and growth of α'; precipitation of a nickel (Ni)- and silicon (Si)-rich G phase, $M_{23}C_6$ carbide, and γ_2 (austenite); and additional precipitation and/or growth of existing carbides at the ferrite/austenite phase boundaries.[17-20] The additional phases provide the strengthening mechanisms that increase strain hardening and local tensile stress. Consequently, the critical stress level for brittle fracture is achieved at higher temperatures.

Phase-boundary separation generally occurs in the high-C steels because of the presence of large $M_{23}C_6$ carbides at the phase boundaries. For CF-8 steels, the phase-boundary carbides form during production heat treatment of the casting. Consequently, the unaged CF-8 steels exhibit low lower-shelf energy and high mid-shelf Charpy transition temperature (CTT) relative to the CF-3 steels. The fracture mode for CF-8 steels in the lower-shelf or transition-temperature regime is predominantly phase-boundary separation.[7,8,12,13] In contrast, the CF-3 steels show a dimpled ductile failure. Fracture by phase-boundary separation is observed in only a few heats of unaged CF-8M steels and depends on whether the material contains phase-boundary carbides.

The effects of material variables on the thermal embrittlement of cast stainless steels have been evaluated. The kinetics and extent of thermal embrittlement are controlled by several mechanisms that depend on material parameters and aging temperature. Materials aged at 450°C (842°F) show significant precipitation of phase-boundary carbides (also nitrides in high-nitrogen steels) and a large decrease in ferrite content of the material.[7,8,12,13] At reactor temperatures, such processes either do not occur or their kinetics are extremely slow. Consequently, data obtained for 450°C (842°F) aging do not reflect reactor operating conditions, and extrapolation of the 450°C data to predict the extent of thermal embrittlement at reactor temperatures is not valid.

The chemical composition, production heat treatment, and ferrite content and spacing of the steel are important parameters in controlling the extent and kinetics of thermal embrittlement. Ferrite morphology strongly affects the extent of thermal embrittlement, whereas material composition influences the kinetics of embrittlement. Small changes in the constituent elements of the cast material can cause the kinetics of thermal embrittlement to vary significantly. The kinetics of thermal embrittlement are controlled by spinodal decomposition of ferrite, and precipitation and growth of phase-boundary carbides. The rate of thermal embrittlement for a specific cast stainless steel depends on the relative contributions of these precipitation processes; activation energies can range from 65 to 230 kJ/mole.

This report presents the correlations for estimating the extent and kinetics of thermal embrittlement of cast stainless steels from known material parameters. The extent of embrittlement is characterized by the room-temperature "normalized" Charpy-impact energy (Charpy-impact energy per unit area). Based on the information available, two methods are presented for estimating the extent of embrittlement at "saturation," i.e., the minimum impact energy that would be achieved for the material after long-term aging. The first method utilizes only the information available in the certified materials test record (CMTR), i.e., chemical composition of the steel. The second method is used when metallographic information on the ferrite morphology is also available, i.e., measured values of ferrite con-

6

tent and mean ferrite spacing of the steel are known. The change in Charpy-impact energy as a function of time and temperature of reactor service is then estimated from the extent of embrittlement at saturation and from the correlations describing the kinetics of embrittlement. The results from Charpy-impact tests and microhardness measurements of the ferrite phase for several heats of cast stainless steel aged up to 30,000 h at 290–400°C (554–752°F) are analyzed to establish the kinetics of thermal embrittlement. A correlation is presented for estimating the activation energy of thermal embrittlement from chemical composition and the aging behavior of the steel at 400°C. Examples for estimating impact strength of cast stainless steel components during reactor service are described.

2 Extent of Embrittlement at Saturation

Charpy-impact data obtained at room temperature indicate that, for a specific heat of cast stainless steel, a saturation value of minimum impact energy is reached after aging for 3,000–10,000 h at 400°C (752°F) or 30,000–60,000 h at 350°C (662°F). The variation of this saturation impact energy C_{Vsat} for different materials can be expressed in terms of a material parameter Φ that is determined from the chemical composition and ferrite morphology of the materials. It is well established that the extent of embrittlement increases with an increase in the ferrite content of cast stainless steel. Furthermore, Charpy-impact data for several heats of CF–8 and CF–8M steels indicate that impact energy decreases with an increase in Cr content, irrespective of the ferrite content of the steel.[23] A better correlation is obtained when the total concentration of ferrite formers (i.e., Cr, Mo, and Si) is considered.[23] A sharp decrease in impact energy occurs when either the Cr content exceeds 18 wt.% or the concentration of Cr+Mo+Si exceeds 23.5 wt.%. The concentration of Ni and Si in the steel, i.e., the elements that promote G–phase formation, also appears to increase the extent of embrittlement of the Mo–bearing CF–8M steels. An increase in the concentration of C or N in the steel also increases the extent of embrittlement because of the contribution to phase–boundary carbides or nitrides and the subsequent fracture by phase–boundary separation.

Based on the amount of information available, two different methods for estimating the material parameter and saturation impact energy are presented. The first method utilizes only the information available in the CMTR, i.e., chemical composition of the material. The second method allows an estimate of saturation impact energy to be obtained when metallographic information on ferrite morphology is also available, i.e., the measured values of ferrite content and mean ferrite spacing of the steel are known.

2.1 Method A – When Only a CMTR Is Available

The "saturation" fracture toughness of a specific cast stainless steel, i.e., the minimum fracture toughness that would be achieved by the material after long-term service, is estimated from the degree of embrittlement at saturation. The degree of embrittlement is characterized in terms of room–temperature "normalized" Charpy-impact energy. The variation of the impact energy at saturation for different materials can be expressed in terms of a material parameter Φ, which is determined from the chemical composition.

The material parameter Φ is estimated from the information available in the CMTR, e.g., chemical composition. The ferrite content is calculated in terms of the Hull's equivalent factors[28]

$$Cr_{eq} = Cr + 1.21(Mo) + 0.48(Si) - 4.99 \tag{1}$$

and

$$Ni_{eq} = (Ni) + 0.11(Mn) - 0.0086(Mn)^2 + 18.4(N) + 24.5(C) + 2.77, \tag{2}$$

where chemical composition is in wt.%. The concentration of N is often not available in the CMTR; it is assumed to be 0.04 wt.% if not known. The ferrite content δ_c is given by the relation

$$\delta_c = 100.3(Cr_{eq}/Ni_{eq})^2 - 170.72(Cr_{eq}/Ni_{eq}) + 74.22. \tag{3}$$

The measured and calculated values of ferrite content for the various heats used in studies at ANL,[7-15] Framatome (FRA),[25] Georg Fischer Co. (GF),[1] Electricité de France (EdF),[23] Central Electricity Generation Board (CEGB),[24] and Electric Power Research Institute (EPRI)[27] are shown in Fig. 1. The chemical composition, ferrite content, and room-temperature Charpy-impact energy of the various materials are given in Tables 1 and 2. For most heats, the difference between the estimated and measured values is ±6% ferrite. The few heats for which the estimated ferrite contents are significantly lower than the measured values generally contain ≥10% Ni.
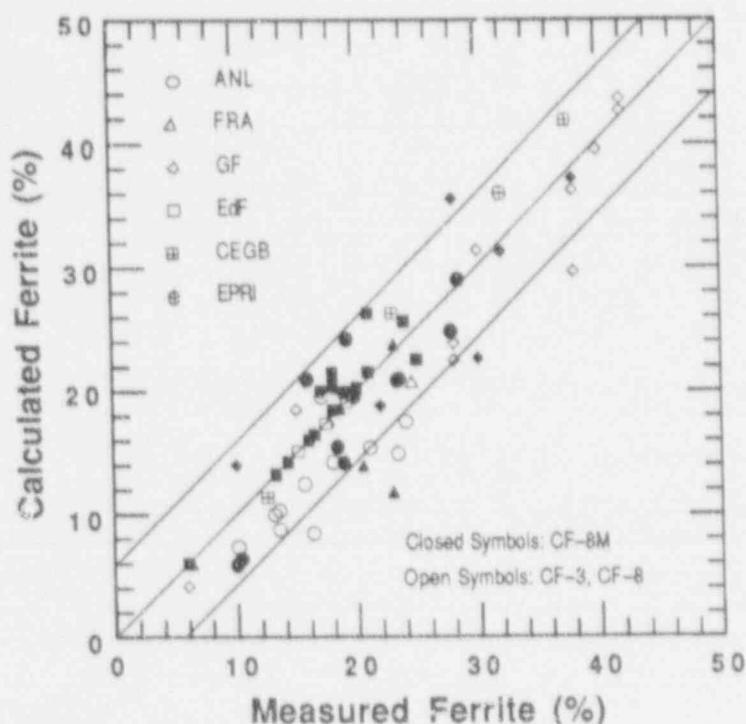
Figure 1. Measured and calculated ferrite contents for various heats of cast stainless steels

Table 2. *Chemical composition and kinetics of thermal embrittlement for Georg Fischer and Framatome heats of cast stainless steels*

	Chemical Composition (wt.%)							C_{Vsat}	Constants			Q
Heat	Cr	Mo	Si	Ni	Mn	C	N	(J/cm²)	β	θ	α	(kJ/mole [kcal/mole])
277	20.5	0.06	1.81	8.13	0.54	0.052	0.010	33.5	0.488	3.65	0.55	88 (21.0)
278	20.2	0.13	1.00	8.27	0.28	0.038	0.030	68.3	0.381	4.05	0.47	63 (15.0)
279	22.0	0.22	1.36	7.85	0.37	0.040	0.032	23.8	0.586	3.21	0.69	92 (21.9)
280	21.6	0.25	1.37	8.00	0.50	0.028	0.038	24.4	0.591	3.30	0.73	87 (20.7)
281	23.1	0.17	0.45	8.60	0.41	0.036	0.053	26.6	0.560	3.76	0.42	93 (22.1)
282	22.5	0.15	0.35	8.53	0.43	0.035	0.040	30.0	0.525	3.73	0.43	98 (23.4)
283	22.6	0.23	0.53	7.88	0.48	0.036	0.032	23.8	0.580	3.65	0.43	83 (19.8)
284	23.0	0.17	0.52	8.23	0.28	0.025	0.037	23.8	0.560	3.71	0.41	87 (20.9)
291	19.6	0.66	1.59	10.60	0.28	0.065	0.054	121.9	0.235	3.89	0.79	77 (18.5)
292	21.6	0.13	1.57	7.52	0.34	0.090	0.039	22.2	0.392	3.08	0.46	99 (23.7)
285	18.8	2.35	0.86	9.49	0.48	0.047	0.039	64.3	0.347	3.76	0.34	82 (19.6)
286	20.2	2.44	1.33	9.13	0.40	0.072	0.062	20.5	0.571	3.11	0.62	106 (25.2)
287	20.5	2.58	0.51	8.46	0.50	0.047	0.033	23.8	0.563	3.52	0.42	92 (21.9)
288	19.6	2.53	1.70	8.40	0.47	0.052	0.022	19.4	0.643	3.02	0.64	106 (25.3)
289	19.7	2.30	1.44	8.25	0.48	0.091	0.032	21.1	0.571	3.32	0.39	90 (21.6)
290	20.0	2.40	1.51	8.30	0.41	0.054	0.050	21.1	0.602	3.49	0.11	81 (19.3)
C	20.7	0.13	1.09	8.19	1.09	0.042	0.035	51.0	0.393	3.30	0.45	83 (19.9)
E	21.0	0.08	0.54	8.47	0.80	0.035	0.051	45.0	0.334	2.63	0.65	133 (31.8)
F	19.7	0.34	1.16	8.33	0.26	0.038	0.026	83.0	0.282	2.45	1.23	176 (41.1)
B	20.1	2.52	0.93	10.56	0.83	0.053	0.042	31.0	0.478	2.55	0.47	129 (30.7)
D	19.2	2.44	0.94	10.32	1.12	0.026	0.063	33.0	0.439	3.30	0.40	90 (21.4)

Different correlations are used to estimate the saturation impact energy of the various grades of cast stainless steel. For CF–3 and CF–8 steels, the material parameter Φ is expressed as

$$\Phi = \delta_c(Cr + Si)(C + 0.4N) \qquad (4)$$

and the saturation value of room–temperature normalized impact energy C_{Vsat} is given by

$$\log_{10}C_{Vsat} = 1.15 + 1.374\exp(-0.0365\Phi). \qquad (5)$$

For the Mo-bearing CF-8M steels, the material parameter Φ is expressed as

$$\Phi = \delta_c Cr(C + 0.4N)(Ni + Si)^2/100 \qquad (6)$$

and the saturation value of room–temperature normalized impact energy C_{Vsat} is given by

$$\log_{10}C_{Vsat} = 1.15 + 1.532\exp(-0.0467\Phi). \qquad (7)$$

In Eqs. 4 and 6, N content can be assumed to be 0.04 wt.% if the value is not known.

9

The saturation values of room–temperature impact energy predicted by Eqs. 4 and 5 and those observed experimentally at ANL, FRA, GF, EdF, CEGB, and EPRI are shown in Fig. 2a. The difference between the predicted and observed values is $<\pm15\%$ for most of the materials. The observed room–temperature impact energy at saturation and values predicted by Eqs. 6 and 7 are shown in Fig. 2b for the data from ANL, FRA, GF, and EdF studies. The difference between observed and predicted values for the CF-8M steel is larger than that for the CF-3 or CF-8 steels. The correlations expressed in Eqs. 4–7 do not include Nb and may not be conservative for Nb-bearing steels.

2.2 Method B – When Metallographic Information Is Available

A common expression for material parameter for the various grades of steel can be obtained when the measured values of ferrite content and mean ferrite spacing of the steel are known. In this case, the material parameter Φ is representative of both the structure and the steel composition and is given by

$$\Phi = \delta_m{}^2(Cr + Mo + Si)(C + 0.4N)Ni\lambda / 10^4, \tag{8}$$

where δ_m is the measured ferrite content (in %) and λ is the mean ferrite spacing (in μm). The saturation value of room–temperature impact energy C_{Vsat} is given by the relation

$$\log_{10}C_{Vsat} = 1.386 + 0.938\exp(-0.0205\Phi). \tag{9}$$

In the field, δ_m would have to be measured with a magne–gage or a ferrite scope (nonsaturation magnetic induction principle) and λ would be determined from metallographic replicas of the actual component. The N content is assumed to be 0.04 wt.% if not known.

Plots of room–temperature impact energy and the material parameter Φ, calculated from Eqs. 8 and 9, are shown in Fig. 3, together with data from studies at ANL, FRA, GF, CEGB, and EPRI. The saturation impact energies predicted from Eqs. 8 and 9 for CF-3 or CF-8 steels are comparable to those estimated from Eqs. 4 and 5; those for CF-8M steel are better than those estimated from Eqs. 6 and 7. As discussed in the previous section, Eq. 8 also does not consider the effects of Nb on embrittlement and, hence, may not be conservative for Nb-bearing cast stainless steels.

3 Kinetics of Embrittlement

3.1 Charpy–Impact Energy

The results from room–temperature Charpy–impact tests on the various experimental and commercial heats, aged up to 30,000 h at 290, 320, 350, 400, and 450°C (554, 608, 662, 752, and 842°F), were analyzed to determine the kinetics of thermal embrittlement. The variation of the Charpy–impact energy C_V (J/cm^2) with time can be expressed as

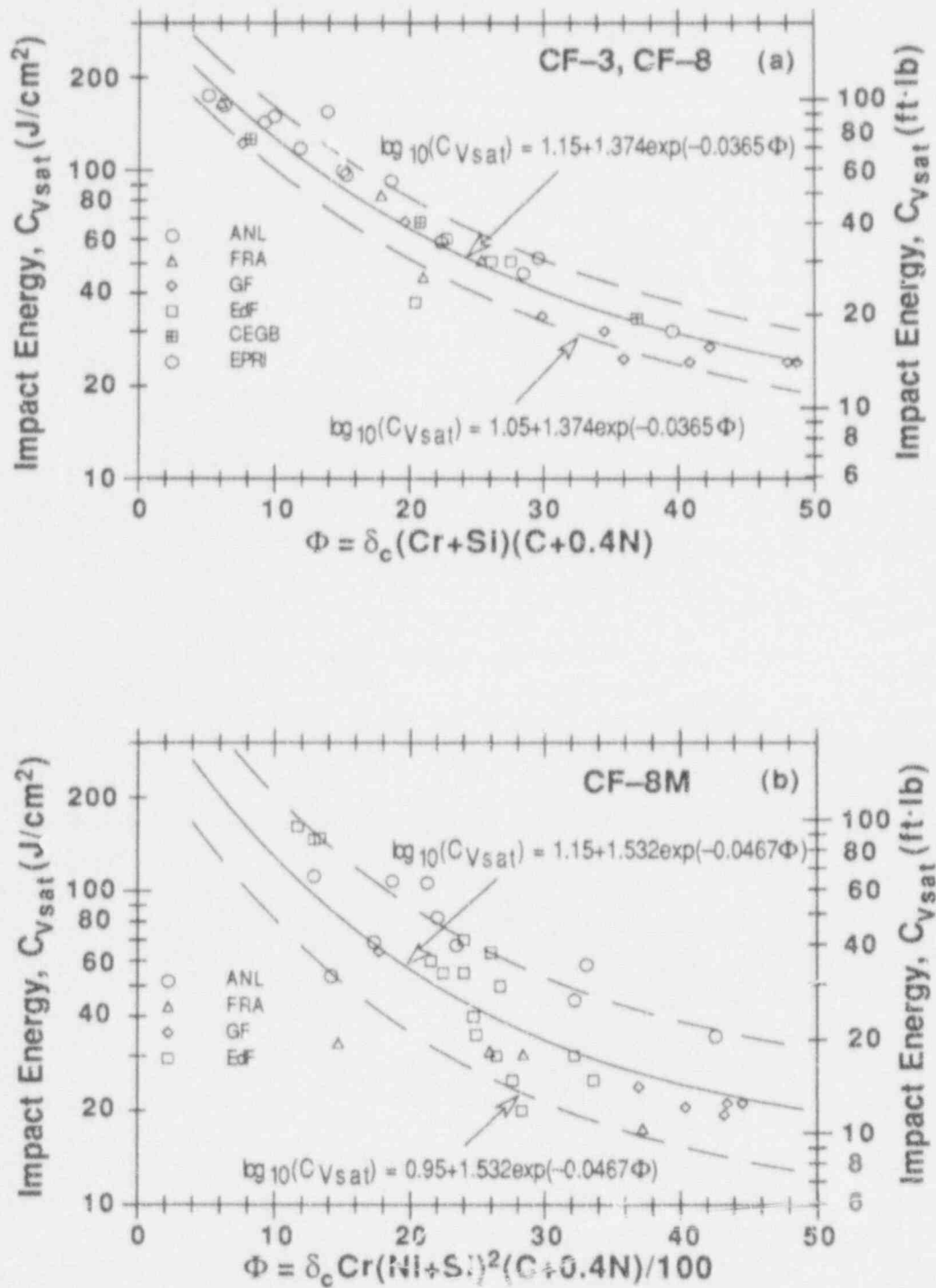$$\log_{10}C_V = \log_{10}C_{Vsat} + \beta\{1 - \tanh [(P - \theta)/\alpha]\}. \tag{10}$$

10

Figure 2. Correlation between room–temperature Charpy–impact energy at saturation and material parameter Φ (method A) for CF–3, CF–8, and CF–8M steels. The dashed lines represent (a) ±26% and (b) ±58% deviation from the predicted values.
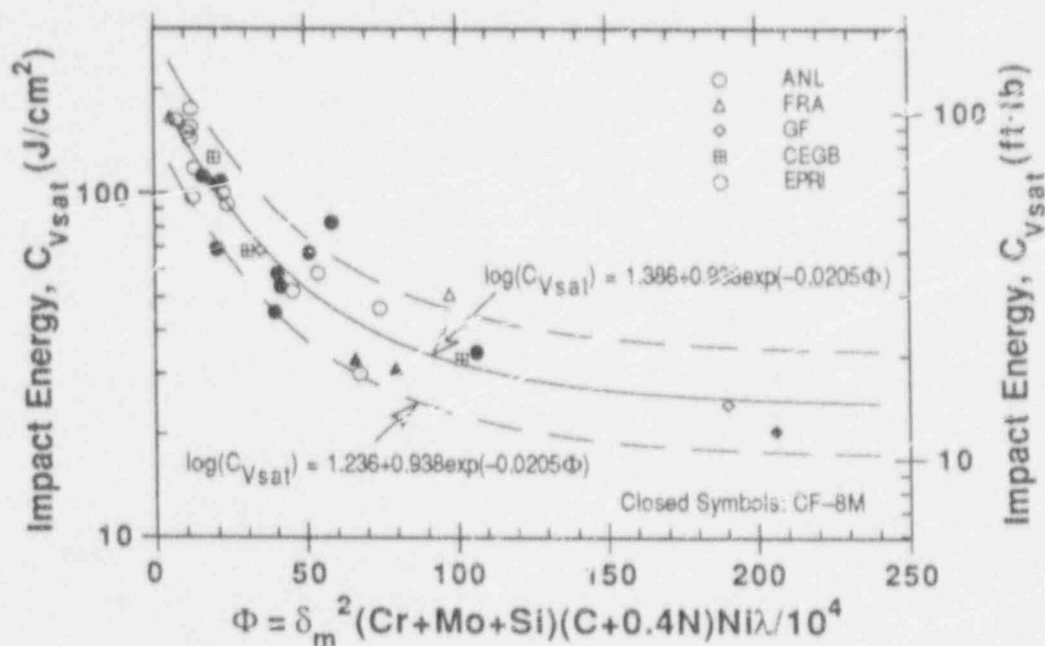
Figure 3. Correlation between room-temperature Charpy-impact energy at saturation and material parameter Φ (method B) for all grades of cast stainless steels. The dashed lines represent ±41% deviation from the predicted values.

where C_{Vsat} (J/cm^2) is the saturation Charpy-impact energy that would be reached after long-term aging, β is half the maximum change in $logC_V$, θ is the log of the time to achieve β reduction in impact energy at 400°C, α is a shape factor, and P is the aging parameter defined by

$$P = \log_{10}[t] - \frac{1000Q}{19.143}\left\{\frac{1}{T_s+273} - \frac{1}{673}\right\},$$ (11)

where Q is the activation energy (kJ/mole) and t and T_s are the time (h) and temperature (°C) of aging. Equation 11 considers aging at 400°C as the baseline aging behavior for the material and parameter P is the log of the aging time at 400°C. The data obtained after 450°C aging are not representative of reactor operating conditions and were therefore excluded from the analysis. Charpy data obtained after 290°C aging often showed no reduction in impact energy even after aging for 30,000 h; instead, a slight increase in impact energy was observed relative to the unaged material. The relatively short-time aging data at 290°C tend to bias the analyses to yield higher values of activation energies; therefore, the short-term aging results at 290°C were also excluded from the analysis for some of the heats. The values of the constants in Eqs. 10 and 11 for the GF and FRA heats are given in Table 2 and for the ANL heats in Table 3.

The constant β can be determined from the initial impact energy of the unaged material C_{Vint} and the saturation impact energy C_{Vsat}, thus

Table 3. *Kinetics of thermal embrittlement for ANL heats of cast stainless steel determined from Charpy-impact energy*

Heat	Material Parameter Φ^a	C_{Vsat} (J/cm^2)	Constants β	θ	α	Q (kJ/mole [kcal/mole]) Average	95% Confidence Limit
47	12.0	174.2	0.063	2.35	1.40	187 (44.7)	73–300 (17.5–71.8) [b]
51	10.8	149.2	0.083	3.00	0.76	221 (52.8)	123–320 (29.3–76.4) [b]
69	12.4	96.9	0.202	3.05	0.93	167 (40.0)	120–215 (28.7–51.3) [b]
59	22.2	96.8	0.166	3.12	1.40	229 (54.7)	156–301 (37.4–72.0)
60	45.5	52.0	0.288	2.95	0.89	227 (54.2)	186–267 (44.4–63.9)
68	74.4	46.4	0.348	3.00	0.74	169 (40.5)	136–204 (32.4–48.2)
P1	53.5	56.7	0.282	2.38	0.75	249 (59.6)	210–289 (50.2–69.1)
63	15.8	111.7	0.155	3.20	1.40	119 (28.4)	67–170 (16.0–40.7)
64	39.4	45.2	0.304	2.75	0.62	156 (37.4)	131–181 (31.4–43.2)
65	40.3	58.5	0.269	2.93	0.94	191 (45.7)	154–228 (36.8–54.6)
66	19.5	106.3	0.149	3.02	1.30	203 (48.4)	125–280 (29.9–66.9) [b]
75	106.4	34.7	0.422	2.76	0.53	146 (34.8)	127–165 (30.3–39.4)
P4	41.5	53.8	0.325	2.95	0.89	143 (34.2)	115–171 (27.6–40.8)

[a] Calculated from Eq. 8.
[b] Standard deviation is large due to a relatively small decrease in impact energy and a large scatter in data.

$$\beta = (\log_{10}C_{Vint} - \log_{10}C_{Vsat})/2. \tag{12}$$

The results for the kinetics of thermal embrittlement indicate that the shape factor α increases linearly with C_{Vsat}. The best fit of the data for the various heats yields an expression

$$\alpha = -0.821 + 0.947\log_{10}C_{Vsat}. \tag{13}$$

C_{Vsat} can be calculated from correlations presented in Section 2 if the chemical composition is known. In practice, the initial impact energy is unlikely to be available. Mechanical-property data indicate that the Charpy-impact energy of cast stainless steels is typically 200 ± 20 J/cm^2; however, it can be as low as 60 J/cm^2 for some steels.[12,15]

3.2 Microhardness Measurements

It is well established that the low-temperature thermal embrittlement of cast duplex stainless steels is primarily due to strengthening of the ferrite by precipitation of Cr-rich α' and other phases. The kinetics of thermal embrittlement were also determined from changes in microhardness of the ferrite phase. Microhardness measurements were made on several heats of cast stainless steel aged up to 30,000 h at 320, 350, and 400°C (608, 662, and 752°F), using a diamond-pyramid indenter with 25-g load. At least 20 measurements were made on each sample.

The changes in microhardness for two heats each of CF-8, CF-8M, and CF-3 steels are shown in Figs. 4–6. The results for GF Heats 278 and 280 (from Ref. 1) are shown in Fig. 7.
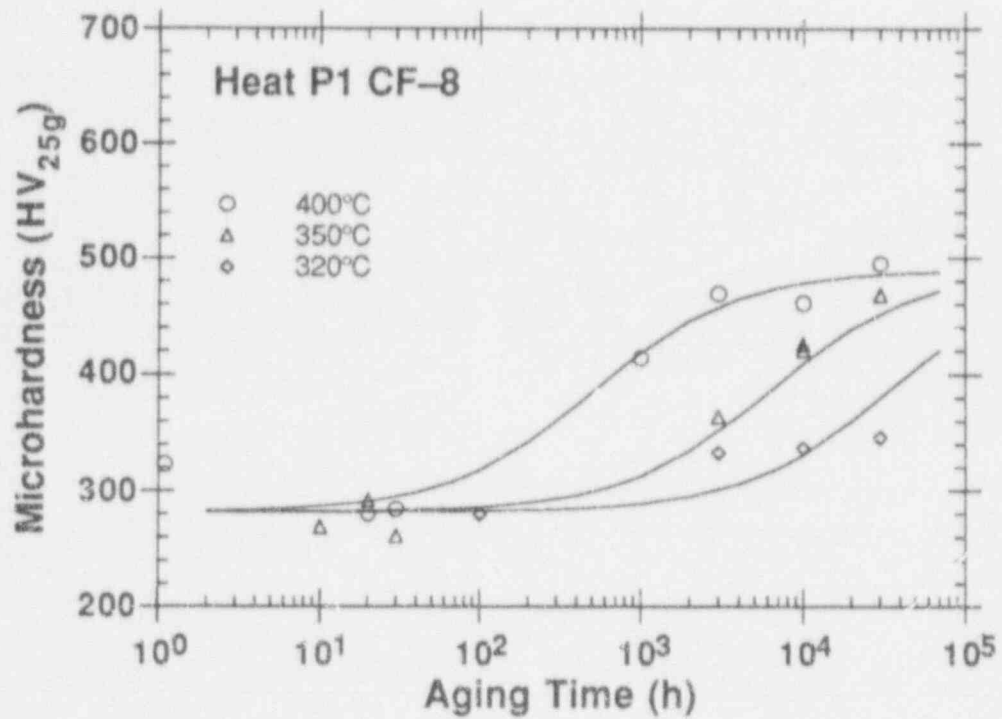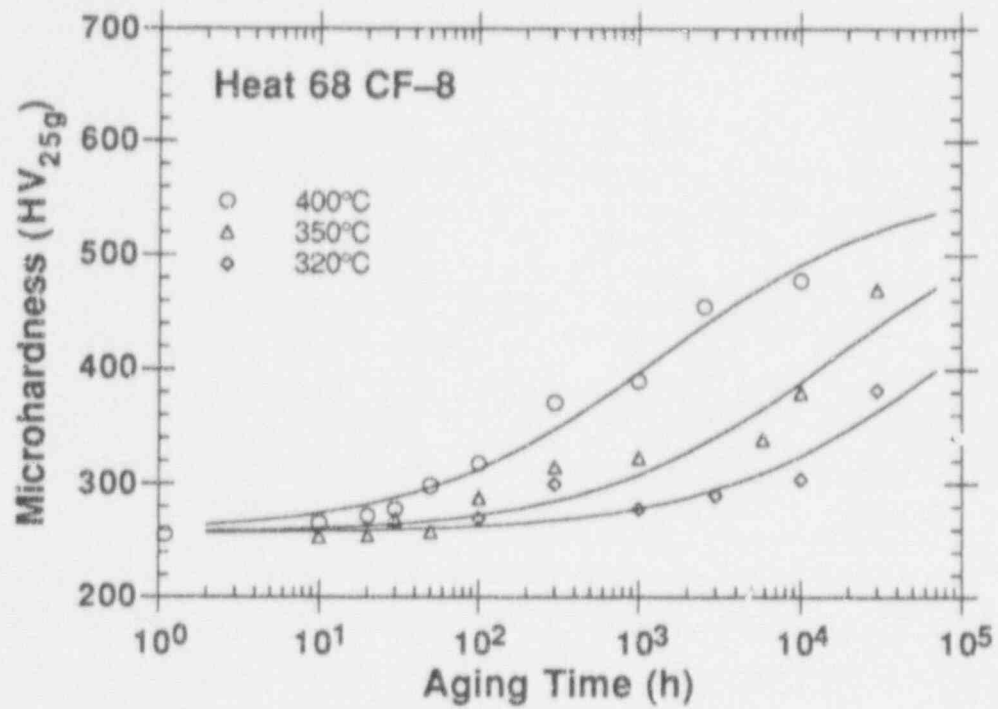
Figure 4.   Change in microhardness of ferrite matrix for aged CF-8 stainless steel
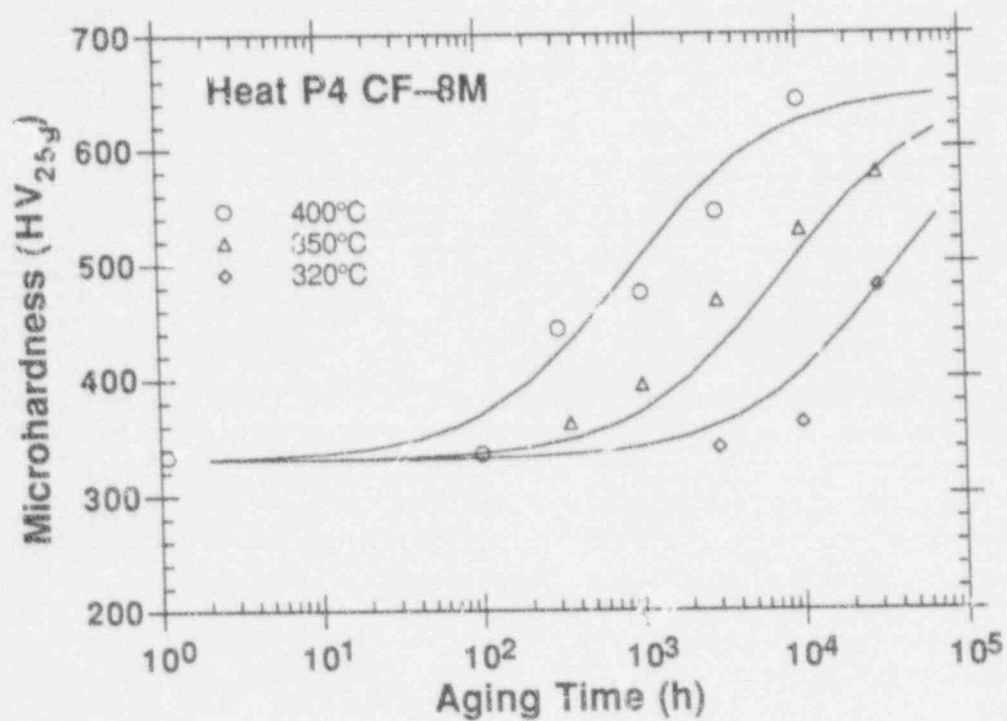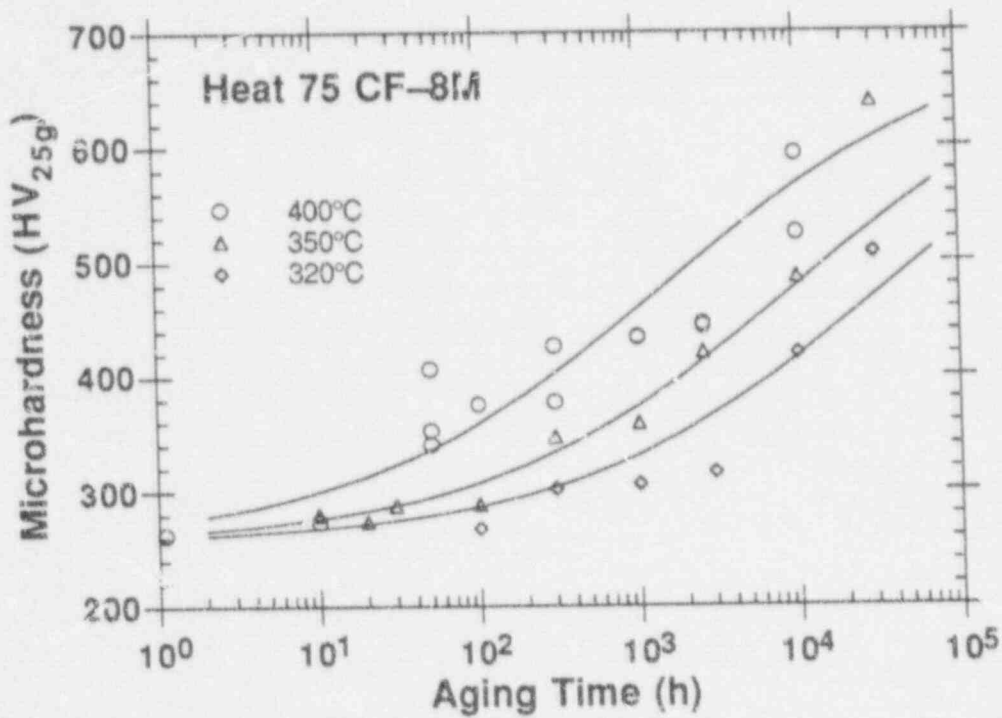
14

Figure 5.   Change in microhardness of ferrite matrix for aged CF–8M
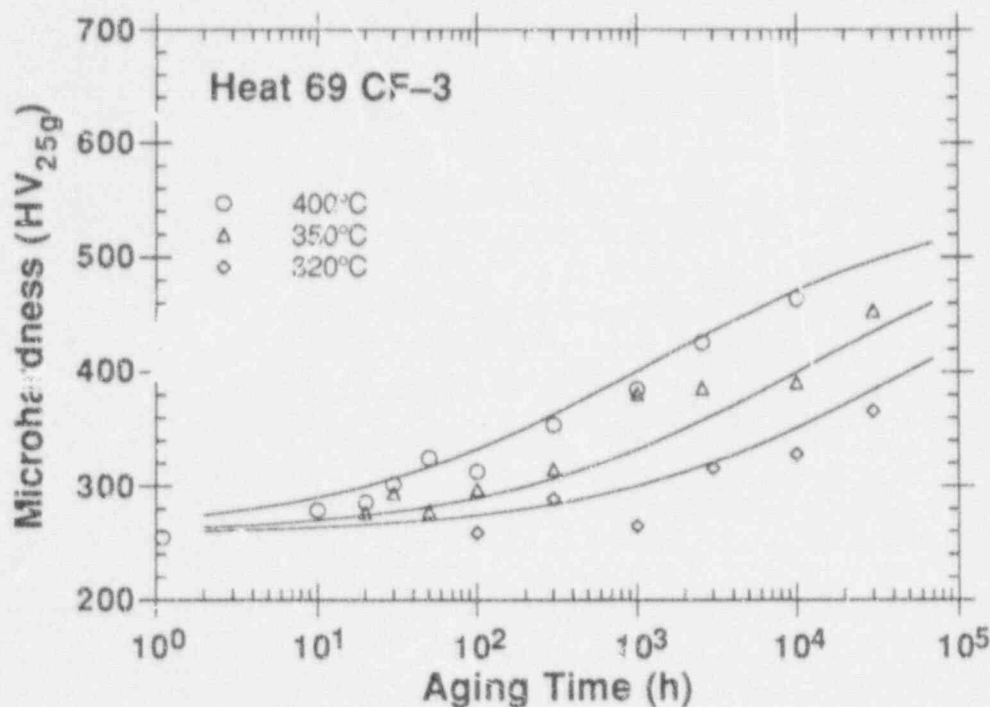   stainless steel

15

Figure 6.   Change in microhardness of ferrite matrix for aged CF–3
             stainless steel

The change in Vickers hardness H can be expressed in terms of a hyperbolic tangent function given by

$$\log_{10} H = H_0 + \beta'(1 + \tanh\,[(P - \theta')/\alpha']),\qquad(14)$$

where H_0 is the initial hardness of the unaged ferrite and constants α', β', θ', and P have the same significance as the constants in Eqs. 10 and 11 for expressing the change in Charpy-impact energy. Values of the constants and activation energies, with 95% confidence limits, are given in Table 4. The results are in very good agreement with the kinetics determined from Charpy-impact data; the activation energy for Heat P1 alone is slightly lower than that determined from Charpy-impact results. An activation energy for thermal embrittlement could not be determined for GF Heat 280 because the change in ferrite hardness for this heat is relatively insensitive to aging temperature (Fig. 7). Similar correspondence between activation energies determined from ferrite hardness and Charpy-impact data has also been observed in CEGB[24] and EdF[23] studies.

The results also indicate that there is no unique correlation between Charpy-impact energy and ferrite hardness. For example, room-temperature Charpy-impact energies at saturation (i.e., fully embrittled condition) for Heats 278, 68, 75, and 280 are 68, 46, 35, and 24 J/cm^2, respectively, while Vickers hardness values are 420, 480, 600, and 440, respectively. The change in ferrite hardness for Heats 280 and 278 is also much lower than that for Heat 75. Ferrite content and morphology of the steel influence the relationship between ferrite hardness and Charpy-impact energy.

16
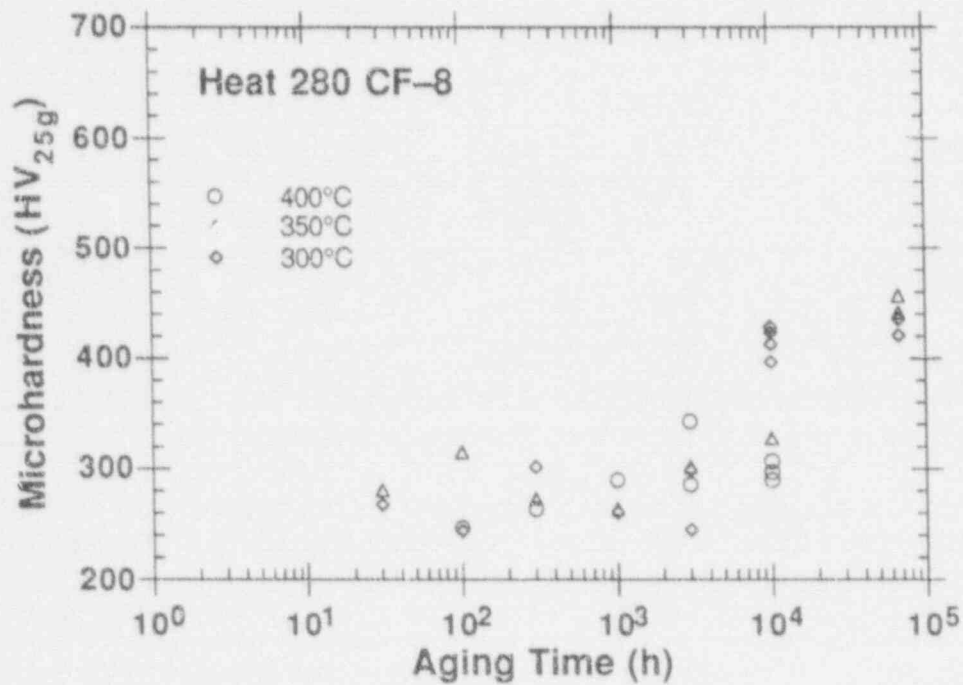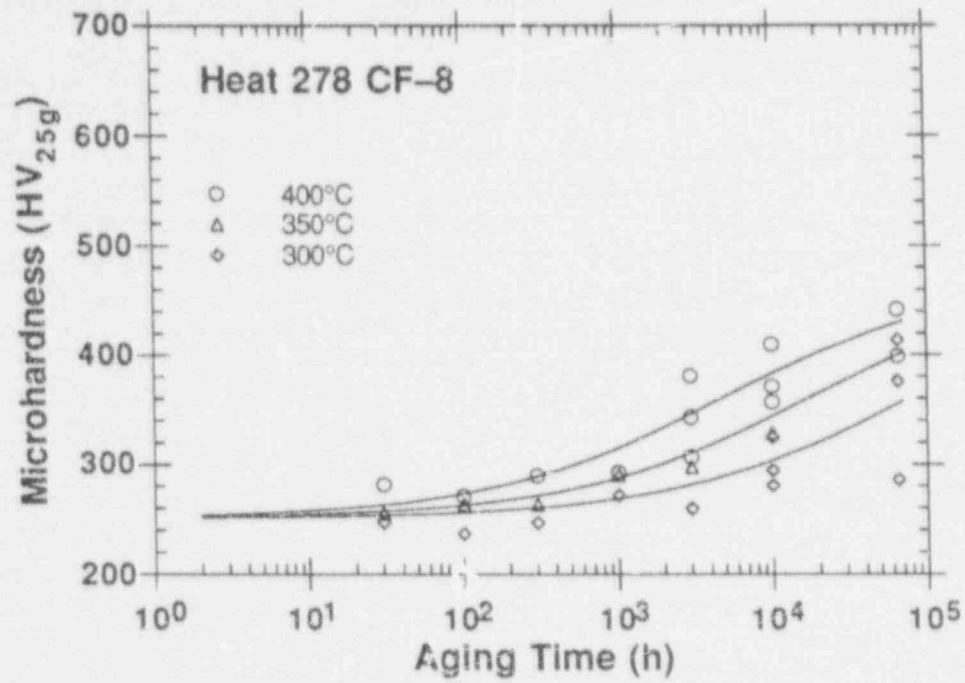
Figure 7. Change in microhardness of ferrite matrix for aged Georg Fischer heats 278 and 280 (Ref. 1)

17

Table 4.   Kinetics of thermal embrittlement of cast stainless steel determined
            from ferrite microhardness

| Heat | H_o | Constants | | | Q [kJ/mole [kcal/mole]] | |
		β'	θ'	α'	Average	95% Confidence Limit
69	2.41	0.168	2.70	2.02	162 (38.7)	120–204 (28.7–48.8)
68	2.41	0.172	2.85	1.53	174 (41.6)	140–207 (33.5–49.5)
P1	2.45	0.120	2.58	0.91	174 (41.6)	112–238 (26.8–56.9)
75	2.41	0.217	2.68	1.97	132 (31.5)	92–172 (22.0–41.1)
P4	2.16	0.185	2.64	1.26	156 (37.3)	112–199 (26.8–47.6)
278	2.39	0.137	3.45	1.56	89 (21.3)	54–124 (12.9–29.6)

3.3 Estimation of Kinetics of Embrittlement

The data from ferrite hardness measurements indicate that thermal embrittlement of cast stainless steels is due to strengthening of the ferrite. Microstructural characterization and annealing studies on thermally aged cast stainless steels show that strengthening of ferrite is caused primarily by spinodal decomposition of the ferrite to form the Cr–rich α' phase.[12,17,18] Consequently, the kinetics of thermal embrittlement should be controlled by the amplitude and frequency of Cr fluctuations produced by spinodal decomposition, i.e., by the size and spacing of the α' phase. Analyses of the changes in the amplitude of Cr fluctuations in aged cast stainless steels by atom probe field ion microscopy (APFIM), yield a high activation energy, i.e., 230±30 kJ/mole associated with Cr diffusion in Fe–Cr alloys.[29] This value corresponds to the upper limit of activation energies determined from ferrite hardness or Charpy–impact data (Tables 2–4). APFIM studies also indicate that the spacing between the Cr fluctuations decreases with decreasing temperature.[30,31] The low activation energies for thermal embrittlement are most likely due to these changes in the spacing of Cr fluctuations at low aging temperatures. The factors that influence the spacing are not well understood.

The aging behavior at 400°C, characterized by the value of θ, varies significantly for the various heats of cast stainless steel. For example, the time of aging at 400°C (752°F) for a 50% reduction in impact energy varies from 200 h (θ=2.3) to 10,000 h (θ=4.0) for the various steels. In general, activation energy increases with a decrease in the value of θ. Consequently, estimation of the change in impact energy suffered by cast stainless steel components (from extrapolation of the high-temperature data to reactor temperatures) would require not only the activation energy for thermal embrittlement of that specific material but also a reference aging behavior of the material at high temperatures, e.g., at 400°C.

The GF heats show very low activation energies for thermal embrittlement, i.e., 65–105 kJ/mole, and their aging behaviors at 400°C are significantly slower than those for the ANL or FRA heats. The values of θ are 3.0–4.0 for the GF and 2.3–3.3 for the ANL or FRA heats (Tables 2 and 3). The constant θ for 12 of the 16 GF heats is >3.3. Such high values of θ are not observed for any other data set. The CEGB data[24] yield θ values of 2.3–2.6 and activation energies 185–215 kJ/mole. The aging behavior of recovery–annealed material from the KRB pump cover plate[4] is also consistent with ANL/FRA/CEGB data (Fig. 8). The recov-

ery-annealed material was aged up to 10,000 h at 320, 350, and 400°C. The results yield an activation energy of 177 kJ/mole and a θ value of 2.3.

A low value of θ was also observed in the EPRI study.[27] For example, the room-temperature Charpy-impact energy decreased from ≈400 to <60 J/cm² after aging at 400°C for only 312 h. Samples of the EPRI heat were aged at ANL for times up to 17,000 h at 350 and 320°C (662 and 608°F). Change in Charpy-impact energy for the material is shown in Fig. 9. The best fit of the data to Eqs. 10 and 11 yields a θ value of 2.1 and an activation energy of ≈225 kJ/mole.

The low activation energies and high θ values are unique to the GF data set. After the production heat treatment of 12 h at 1010 or 1050°C (1850 or 1922°F) and water-quenching, the GF heats were given a second heat treatment of 4 h at 1050°C and then water quenched. GF Heat 280 was also tested in the production heat treatment condition (designated as Heat 280N).[1] The effect of the second heat treatment is reflected clearly in the aging behaviors of Heats 280 and 280N; the θ values for Heats 280 and 280N are 3.3 and 2.5, respectively. Activation energy for Heat 280N is ≈20% higher than for Heat 280.[1] These results suggest that the differences in the aging behavior at 400°C (752°F) and the kinetics of thermal embrittlement of cast stainless steel are most likely caused by the production heat treatment and possibly the casting process, both of which affect the ferrite composition and microstructure.

Based on microstructural studies conducted earlier in this program, a mechanistic correlation has been proposed for estimating the activation energy for thermal embrittlement regardless of the grade of material, range of chemical composition, fabrication process, and
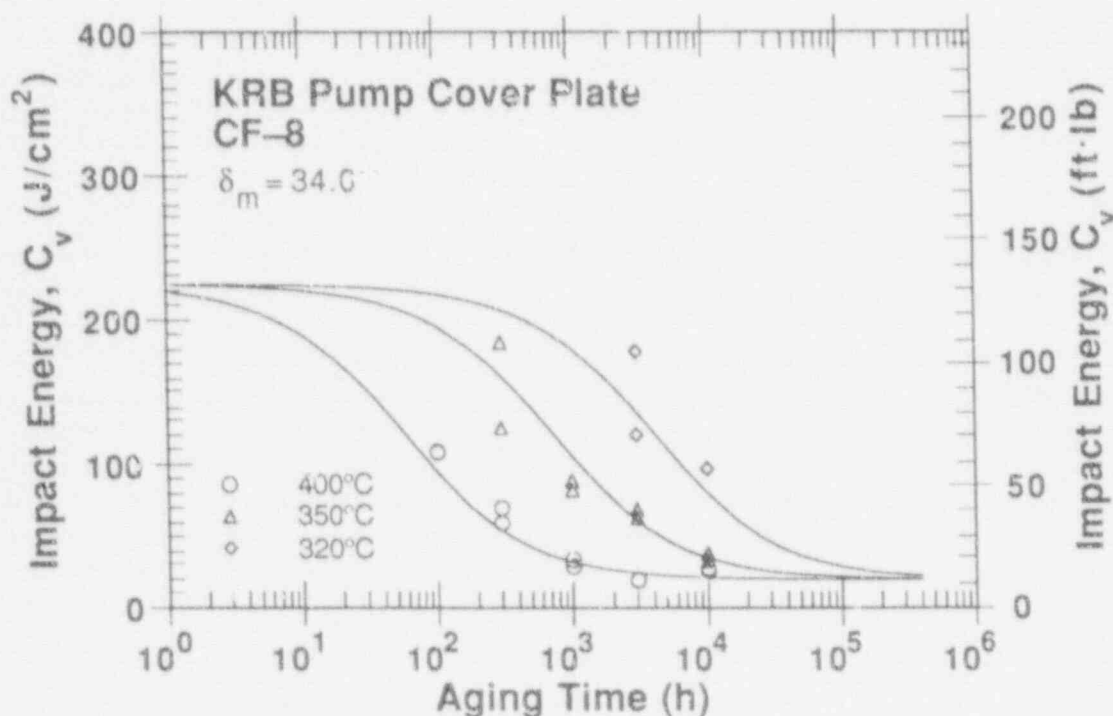
Figure 8.   Change in Charpy-impact energy of annealed KRB pump cover plate material aged at 320, 350, and 400°C

19
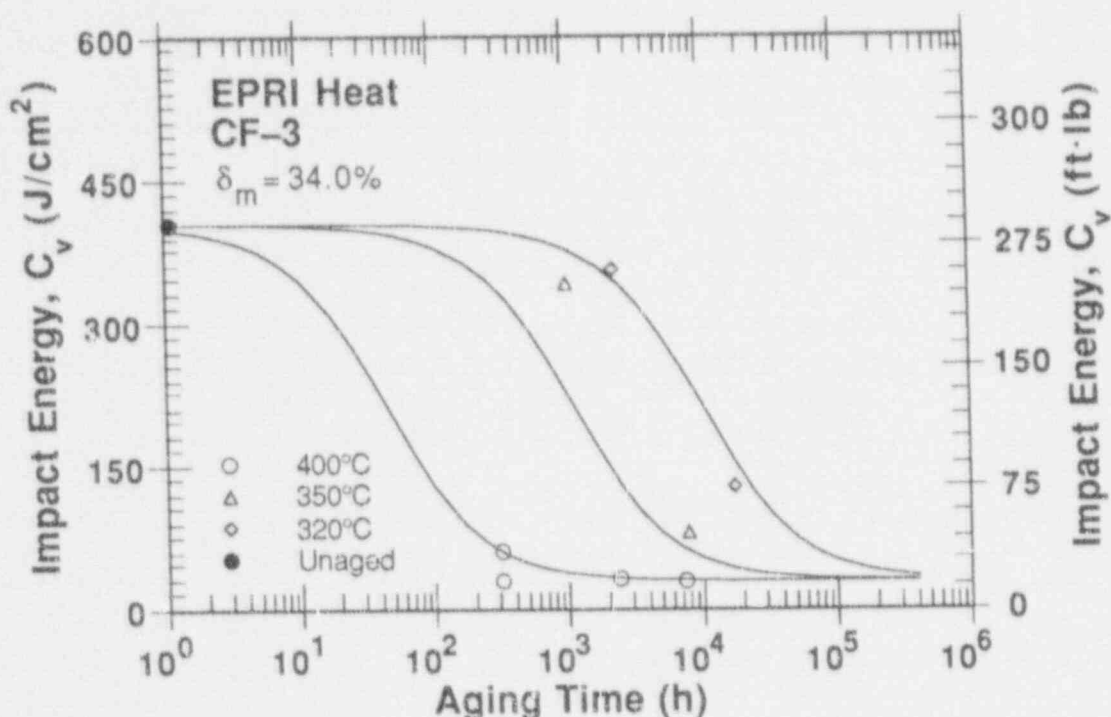
Figure 9. *Change in Charpy–impact energy of EPRI heat aged at 320, 350, and 400°C*

thermomechanical history of the material.[18-20] The activation energy for thermal embrittlement is estimated from the volume fraction of G phase in the ferrite after aging the material for ≈30,000 h at 400°C. Separate correlations are proposed for cast materials in which a large fraction of the ferrite/austenite boundaries is covered with carbides and for those without the phase–boundary carbides. The premise is that the overall activation energy for thermal embrittlement is controlled by the kinetics of spinodal decomposition, the synergistic effects of G–phase precipitation in ferrite, and carbide precipitation at phase boundaries. Spinodal decomposition is slower in materials that show significant G–phase precipitation or Ni–Si clustering, because Ni is depleted from the ferrite matrix. Such effects are more pronounced at 400°C aging, so that the activation energy of thermal embrittlement is lower than the ≈230 kJ/mole value associated with spinodal decomposition in binary Fe–Cr alloys. A schematic representation of the model is shown in Fig. 10. The lines correspond to the aging time required at different temperatures to achieve half the maximum decrease in Charpy–impact energy for the three proposed metallurgical processes. The kinetics of thermal embrittlement when controlled only by spinodal decomposition are represented by the solid line. Activation energy is decreased when G–phase precipitation and Ni–Si clustering accompany spinodal decomposition (as represented by the dash/dot line in Fig. 10). Precipitation of phase–boundary carbides increases the activation energy, as represented by the dashed line.

The data on the kinetics of thermal embrittlement of cast stainless steels are in general agreement with this model, i.e., cast materials with significant G–phase precipitation show low activation energies of thermal embrittlement. Furthermore, in Fig. 10 the log of the time at 400°C is θ in Eq. 10. The model indicates that θ should be high for cast materials that show low activation energy for thermal embrittlement. The GF data set with low

Temperature (°C)
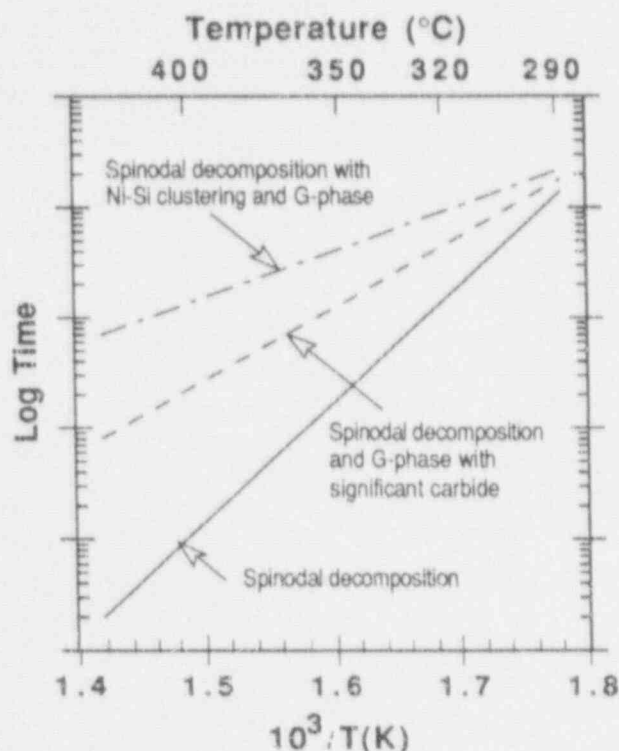
Figure 10. Schematic illustration of kinetics of
thermal embrittlement

activation energies and high θ values corresponds to the dash/dot line, the CEGB data set with high activation energies and low θ values corresponds to the solid line, and the FRA and ANL data sets fall between the two cases. Also, the GF Heats 278, 280, and 286 and ANL Heats 63 and P4 (θ >3.0) show significant G-phase precipitation; ANL Heats 51, 56, 60, 64, 65, and P1 (θ = 2.7–2.9) show some; and none of the CEGB heats (θ <2.6) show G phase.[17-19,31] However, several FRA heats do not follow the above trend. For example, FRA Heats B (θ ≈ 2.6) and C (θ = 3.3) show significant G-phase precipitation, and the volume fraction of G phase is greater in Heat B than in Heat C.[32] However, the activation energy is greater and θ is smaller for Heat B than for Heat C (Table 2). Also, the value of θ for Heat B is comparable to that of the CEGB heats and some ANL heats, but the activation energy for Heat B is much lower than for CEGB or ANL heats. Similar inconsistencies exist for the kinetics and microstructural data for FRA Heat L.[25,33]

The model proposes that depletion of Ni from the ferrite matrix due to G-phase precipitation slows spinodal decomposition and the apparent activation energy is low because G-phase precipitation is more pronounced at 400°C than that at lower temperatures. However, the kinetics of reembrittlement of recovery-annealed materials do not support this argument. Annealing of fully embrittled material for 1 h at 550°C (1022°F) and water-quenching dissolves the α' precipitates, while the G-phase is not affected.[17,18] Therefore, thermal aging of the recovery-annealed material should yield high values of activation energy because G-phase precipitates are already present in the matrix. The reembrittlement of recovery-annealed CF-3, CF-8, and CF-8M steels is compared with their initial aging behavior in Fig. 11. The recovery-annealed materials were first aged for 10,000 h at 400°C, i.e., they were fully embrittled, prior to the annealing treatment of 1 h at 550°C and then

21
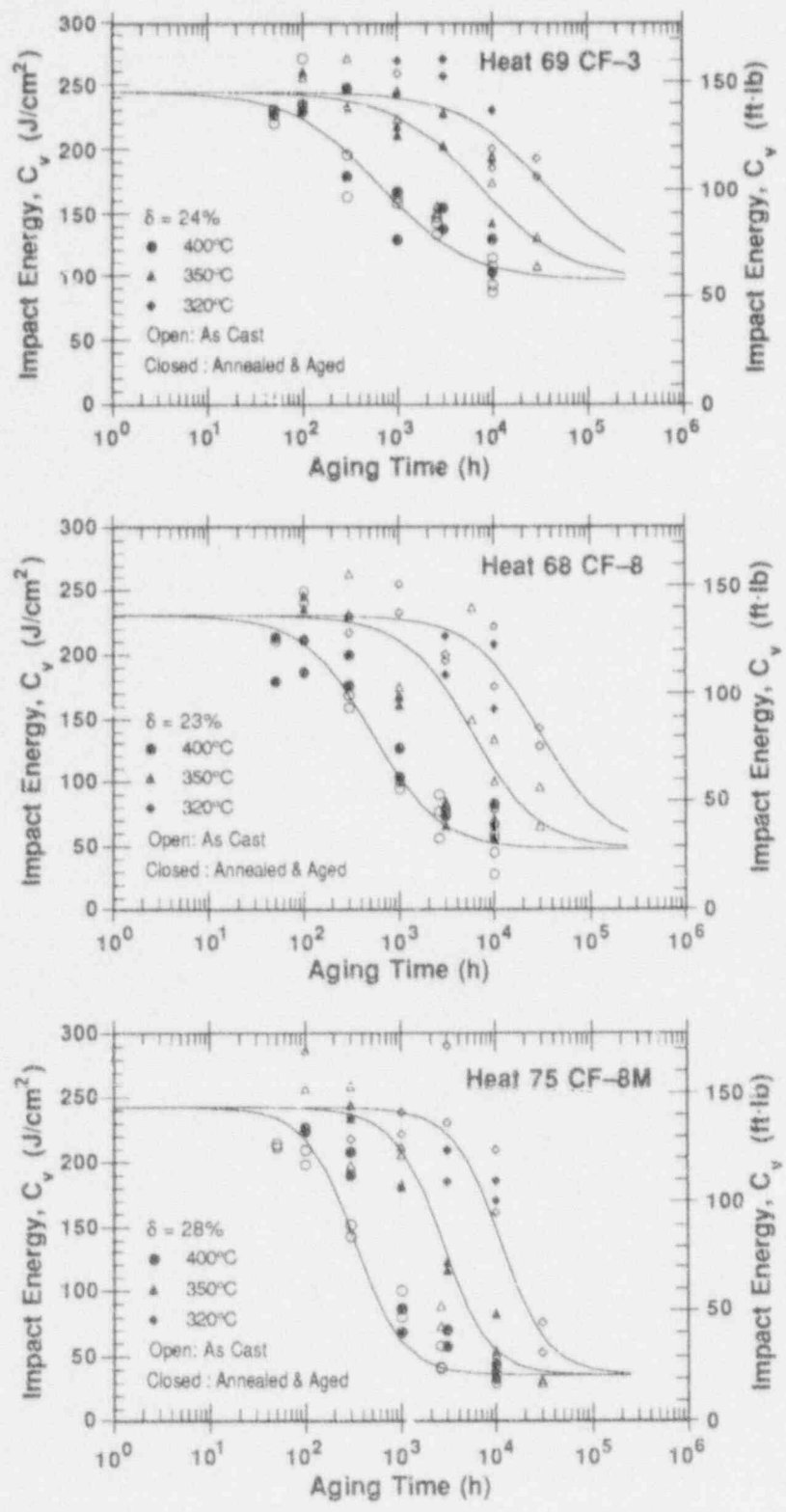
Figure 11. *Effect of thermal aging on room-temperature impact energy of unaged and recovery-annealed CF-3, CF-8, and CF-8M steel. Solid lines represent aging behavior of unaged materials.*

water-quenched. The kinetics of thermal embrittlement for the two materials are virtually identical. The Charpy transition curves for the recovery-annealed materials aged for 10,000 h at 400°C are also essentially the same as those prior to the annealing treatment.[14] The activation energies for thermal embrittlement of Heats 68, 69, and 75 are 168±37, 167±48, and 146±21 kJ/mole, respectively (Table 3). The Charpy data for reembrittlement of recovery-annealed Heats 68, 69, and 75, respectively, yield activation energies of 122±41, 176±49, and 130±28 kJ/mole, i.e., the kinetics of reembrittlement of Heat 69 are comparable and those of Heats 68 and 75 are slightly faster than the kinetics of thermal embrittlement of the unaged materials. However, there is significant overlap in the 95% confidence limits between the values obtained for unaged and recovery-annealed materials. These results suggest that G-phase precipitation in itself is not the cause for changes in the kinetics of embrittlement. Instead both G-phase precipitation and the kinetics of thermal aging are controlled by a fundamental set of material variables, e.g., the composition and microstructure of the ferrite produced after the production heat treatment.

The microstructure-based model also postulates that a high Si content promotes G-phase precipitation and Ni-Si clustering and therefore leads to low activation energy.[20] Figure 10 indicates that this should also result in higher values of θ. Table 2 shows that GF Heats 281, 282, 283, 284, and 287 contain <0.5 wt.% Si, while the others contain >1.3 wt.% Si. Because the casting processes and heat treatments are essentially the same for these heats, the low-Si heats should yield higher activation energies and low values of θ. In all cases, θ values are higher for the low-Si heats and activation energies are not significantly different than those for the high-Si heats. Similar inconsistencies are observed for the ANL and FRA data sets. These results suggest that high Si content is not the only condition for precipitation of G phase.

Another factor that may influence the kinetics of thermal aging is twinning of the ferrite as a mode of deformation for cast duplex stainless steels. The ferrite matrix typically contains ≈26 wt.% Cr and ≈5 wt.% Ni. Deformation twins in ferrite are observed at temperatures up to 300°C (572°F) in thermally aged Fe-Cr alloys containing >4 wt.% Ni.[34-36] Addition of Mo to Fe-Cr alloys also promotes twinning.[34,36] It has been proposed that the depletion of Ni from the ferrite matrix due to G-phase precipitation may change the frequency of twinning and, thus, influence the kinetics of thermal embrittlement.[13] Polished sections of broken Charpy-impact specimens from ≈15 heats of cast stainless steel were examined to investigate the possible role of twinning on the kinetics of thermal embrittlement. A high frequency of twinning was observed in only a few of the heats, e.g., ANL Heat P1, GF Heat 280, EPRI heat, and KRB pump cover plate material (Fig. 12). The other heats, e.g., Heats 47, 69, P2, 60, 68, 63, 64, 75, and P4, contained few or no deformation twins. The presence or amount of twinning shows no correlation with either test temperature or material and aging conditions. The only common factor among the heats that show twinning is ferrite morphology, viz., the ferrite islands are much larger than in the other heats. These results indicate that ferrite twinning has no effect on the kinetics of thermal embrittlement, although it may influence the extent of thermal embrittlement.

Expressions for the activation energy for the thermal embrittlement process in terms of the chemical composition of the cast material are needed to predict component behavior. The earliest correlation, proposed by Framatome,[25] was based on the GF data[1] for 16 heats of cast stainless steel. Activation energy was expressed as a function of the concentrations (wt.%) of Cr, Mo, and Si in the steel:
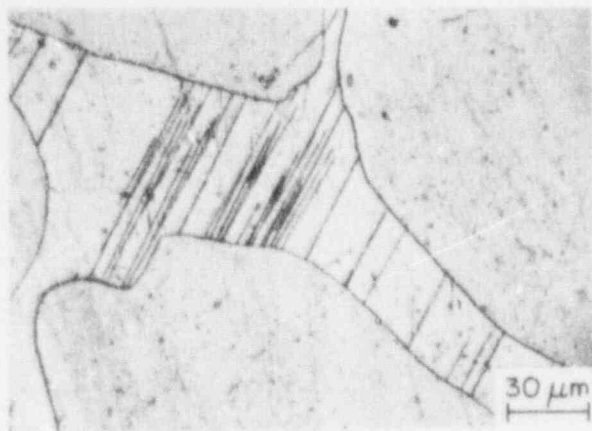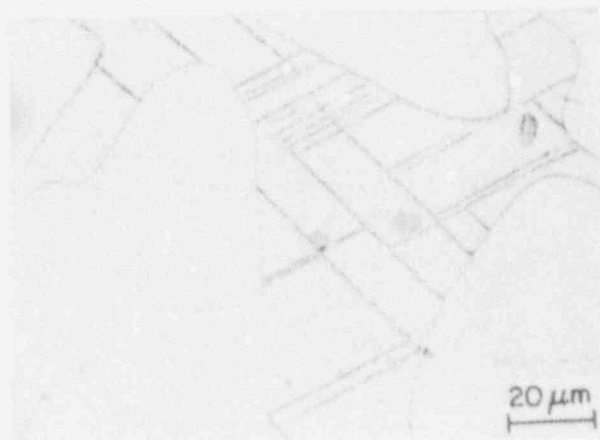
GF Heat 280
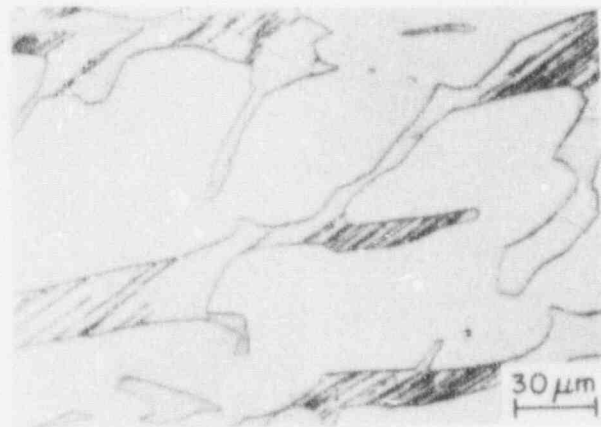
EPRI heat
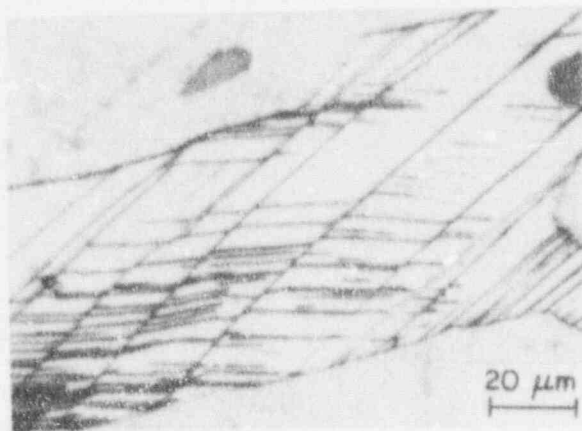
ANL Heat P1

KRB pump cover plate

Figure 12. *Deformation twins in broken Charpy-impact test specimens of unaged and aged cast stainless steels tested at room temperature*

$$Q \text{ (kJ/mole)} = -182.6 + 19.9 \text{ Si} + 11.08 \text{ Cr} + 14.4 \text{ Mo}. \tag{15}$$

The activation energy calculated from Eq. 15 for thermal embrittlement ranges from 65 to 105 kJ/mole for the various grades of cast stainless steel. However, the estimated activation energies for ANL and CEGB heats are a factor of 2 lower than the experimental values. The GF data set covers a relatively narrow range of compositions, and the ferrite contents of most heats are above 30% and therefore not representative of compositions defined by ASTM Specification A 351.

Subsequent correlations developed by ANL[12,13] were based on a larger data base. Two separate correlations were proposed: one for the ANL data[7–15] and FRA data[25] (15 heats), given by
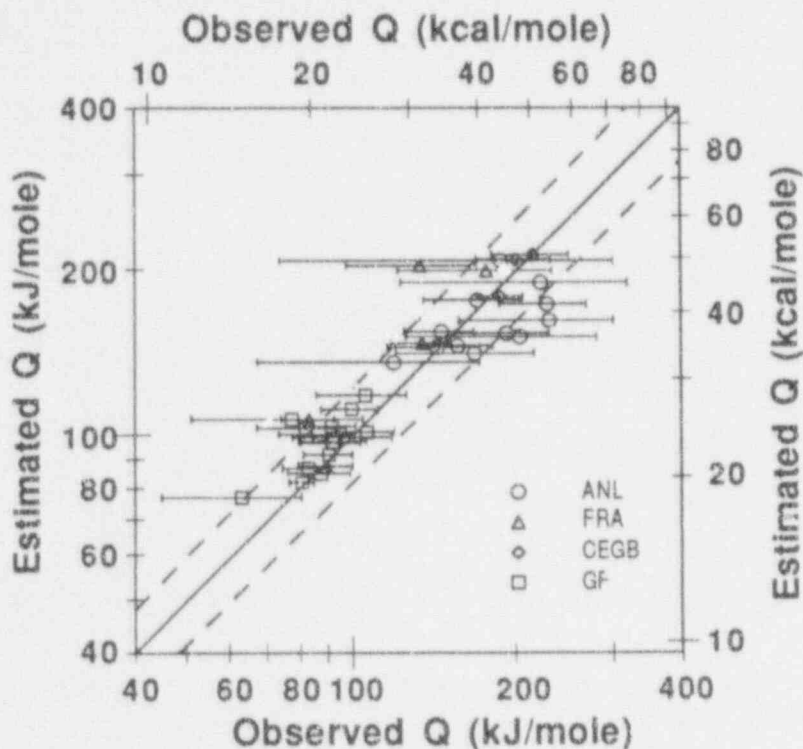
24
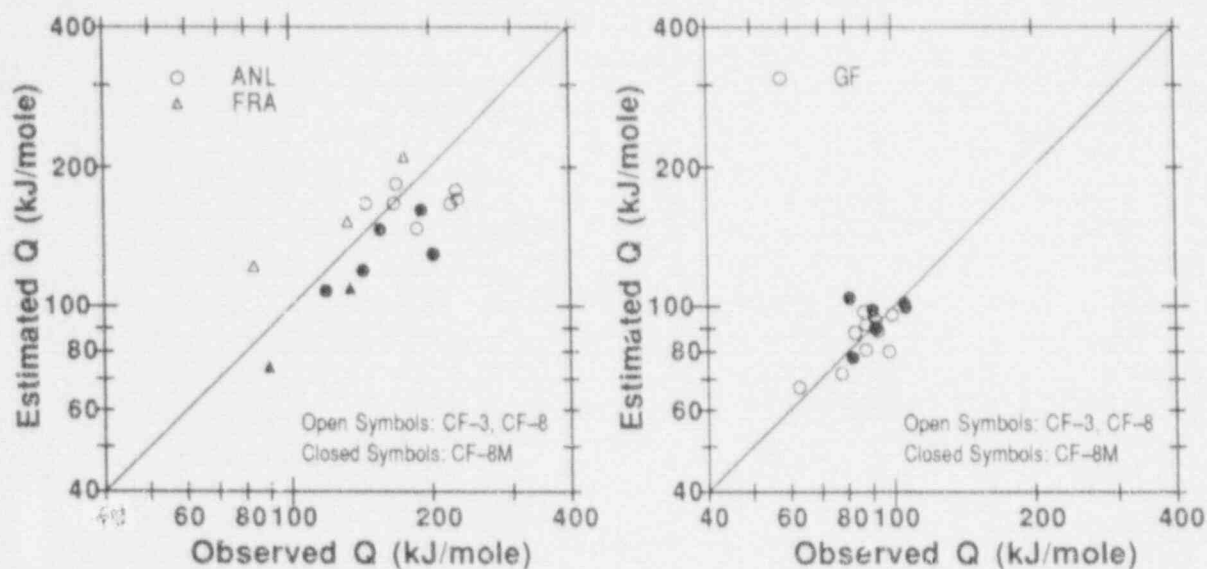
Figure 13. Observed activation energy and values predicted from Eqs. 16 and 17 for thermal embrittlement of cast stainless steels

$$Q \; (kJ/mole) = 90.54 + 9.62 \; Cr - 8.12 \; Ni - 7.53 \; Mo$$
$$+ \; 20.59 \; Si - 123.0 \; Mn + 317.7 \; N, \tag{16}$$

and the other for the GF data[1] (16 heats), given by

$$Q \; (kJ/mole) = -66.65 + 6.90 \; Cr - 5.44 \; Ni + 8.08 \; Mo$$
$$+ \; 17.15 \; Si + 44.1 \; Mn + 297.1 \; N, \tag{17}$$

where the constituent elements are given in wt.%. Observed and predicted activation energies for the two data sets are plotted in Fig. 13. For a specific material composition, the activation energies predicted from Eqs. 15 and 17 are comparable, while those from Eq. 16 are higher. The ANL data used in developing the correlations represented only the high-temperature aging; the results for long-term aging (i.e., 30,000 h) at 290 or 320°C (554 or 608°F) were not included in the analyses. Thus, the calculated activation energies primarily represent the kinetics of thermal embrittlement at 350–450°C (662–842°F). These values are 15 to 20% lower than those determined from aging data at 290–400°C (554–752°F), see Table 3.

The Charpy data for the kinetics of thermal embrittlement have been reanalyzed to develop a general correlation for activation energy that would be applicable for all chemical compositions within the ASTM Specification A 351 and valid for the entire temperature range of extrapolation, i.e., 280–400°C (536–752°F). In this new correlation activation energy for thermal embrittlement was expressed in terms of both chemical composition and the constant θ (defined in Eq. 10) to incorporate the possible effects of heat treatment and the casting process on the kinetics of thermal embrittlement. The best fit of the data from ANL, FRA, GF, and CEGB studies (36 heats) yields the expression

Figure 14. Observed activation energy and values predicted
from Eq. 18 for thermal embrittlement of cast
stainless steels

$$Q \text{ (kJ/mole)} = 10 \, [74.06 - (7.66 - 0.46 \, I_1) \, \theta - 4.35 \, Si + 1.38 \, I_2 \, Mo$$
$$- 1.67 \, Cr - (2.22 + 3.56 \, I_1) \, Mn + (108.8 - 75.3 \, I_1) \, N], \tag{18}$$

where the indicators $I_1 = 0$ and $I_2 = 1$ for CF-3 or CF-8 steels and assume the values of 1
and 0, respectively, for CF-8M steels. The estimated and observed values of Q for the ANL,
FRA, CEGB, and GF heats are plotted in Fig. 14. The error bars represent 95% confidence
limits for the observed values of Q. The dashed lines represent a ±20% range. The pre-
dicted values are within the 95% confidence limits for all the heats. Equation 18 is appli-
cable for compositions within the ASTM Specification A 351, with an upper limit of 1.2
wt.% for Mn content. Actual Mn content is used up to 1.2 wt.% and is assumed to be 1.2 for
steels containing >1.2 wt.% Mn. Furthermore, the values of Q predicted from Eq. 18
should be between 65 kJ/mole minimum and 250 kJ/mole maximum; Q is assumed to be
65 kJ/mole if the predicted values are lower and 250 kJ/mole if the predicted values are
higher.

The correlation is in qualitative agreement with the microstructural and mechanical-
property data. For example, an increase in the value of θ decreases the activation energy, as
expected. The contributions of Ni, Si, Mo, and Mn are consistent with their effect on G-
phase precipitation. These elements should promote precipitation of G phase, and hence
the coefficients for these elements should have a negative sign because activation energy for
thermal embrittlement is low for steels that show G-phase precipitation. The coefficient of

Mo alone has a positive sign. An increase in C or N in the steel will promote carbide or nitride precipitation and thus increase the activation energy. The positive sign of the coefficient for N agrees with this behavior. However, the correlation with C content in the steel was poor and the term was omitted from the expression.

4 Estimation of Impact Energy

The room-temperature Charpy-impact energy of a specific cast stainless steel can be estimated from the correlations in Sections 2 and 3. Impact energy at saturation C_{Vsat} is determined from the chemical composition of the cast material. The saturation value represents the minimum impact energy that would be achieved by the material after long-term aging. Estimation of the decrease in impact energy as a function of time and temperature of service requires additional information, namely, the initial impact energy of the unaged material and the aging behavior at 400°C (752°F), i.e., the value of constant θ.

The estimated and observed impact energies for some of the ANL, FRA, and GF heats aged at temperatures between 300–350°C (572–662°F) are shown in Figs. 15 and 16. For each heat, the impact energy at saturation was first determined from Eqs. 1–7, i.e., Method A. The activation energy for thermal embrittlement was obtained from Eq. 18; observed values of θ were used for all the heats. Then the change in impact energy with time and temperature of aging was estimated from Eqs. 10–13. The estimated change in impact energy shows good agreement with the observed aging behavior for most of the heats. The shape factor estimated from Eq. 12 is low for a few heats, e.g., Heat 286. Thus, the predicted decrease in impact energy is slower than that observed. For some heats, the estimated C_{Vsat} is higher than the observed value, e.g., Heats P4 and B. Such discrepancies are caused by underestimation of the ferrite content of the steel. A more accurate estimate of C_{Vsat} can be obtained from Eqs. 8 and 9. Generally, conservative values for C_{Vsat} can be obtained by using the lower-limit expressions for Eqs. 5 and 7, i.e., the lower curves shown by the dashed line in Figs. 2 and 3.

Values of θ are not available for cast stainless steel components in the field, and can only be obtained by aging archive material for 5,000 to 10,000 h at 400°C (752°F). Parametric studies show that the aging response at reactor temperatures is relatively insensitive to the values of θ. Varying θ between 2 and 4 results in essentially the same aging behavior at 300°C (572°F). The differences in estimated aging behavior at 280 or 330°C (536 or 626°F) for values in the range of interest are minimal, and a median value of 2.9 for θ can be used to estimate thermal embrittlement at reactor temperatures, i.e., 280–330°C. With an assumed value of 2.9 for θ, estimations of fracture toughness before saturation will be non-conservative for service temperatures >330 and <280°C. Charpy-impact tests have been conducted on reactor-aged components from the Shippingport reactor to benchmark the laboratory data and validate these correlations.[37]

5 Conclusions

The data from Charpy-impact tests and microhardness measurements of the ferrite phase for several heats of cast stainless steel aged up to 30,000 h at 290–400°C (554–752°F) have been analyzed to establish the kinetics of thermal embrittlement. Aging
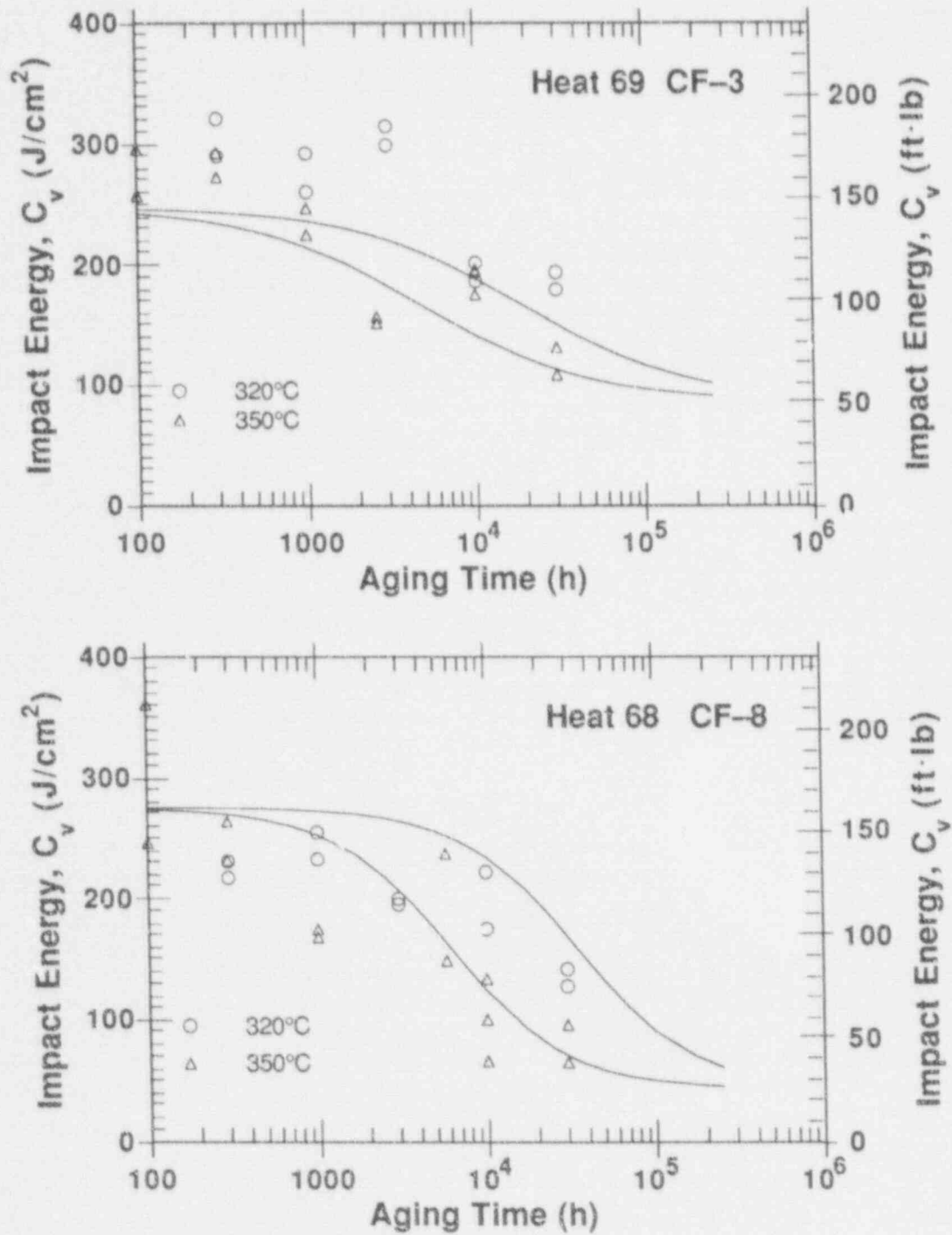
Figure 15. Observed and estimated room-temperature Charpy-impact energy for aged CF-3 and CF-8 cast stainless steels
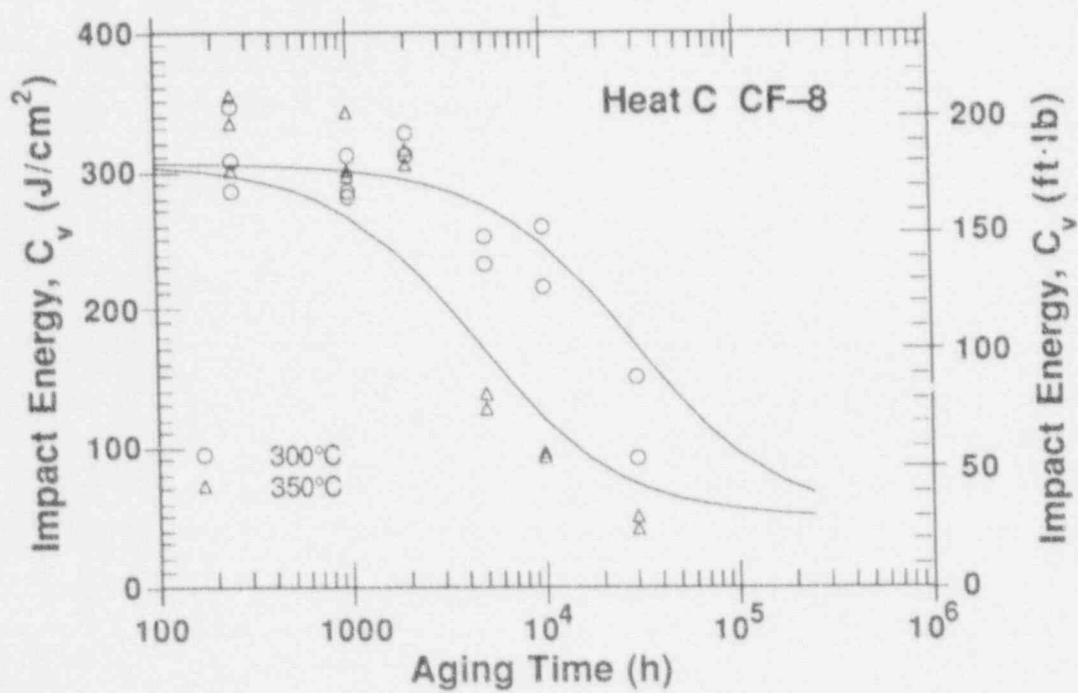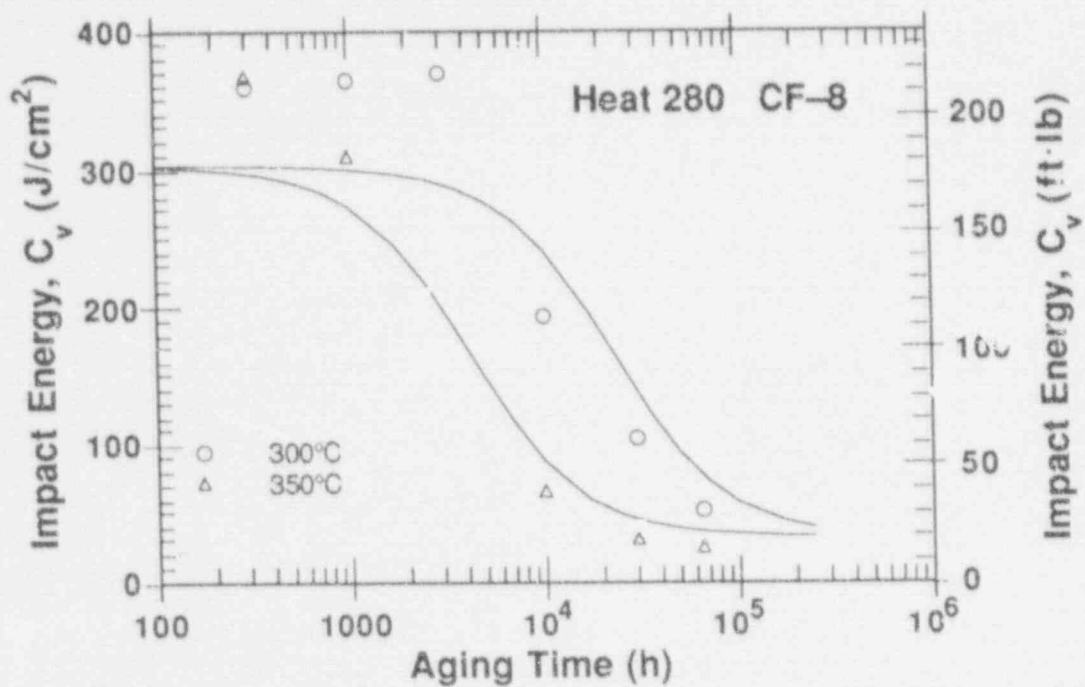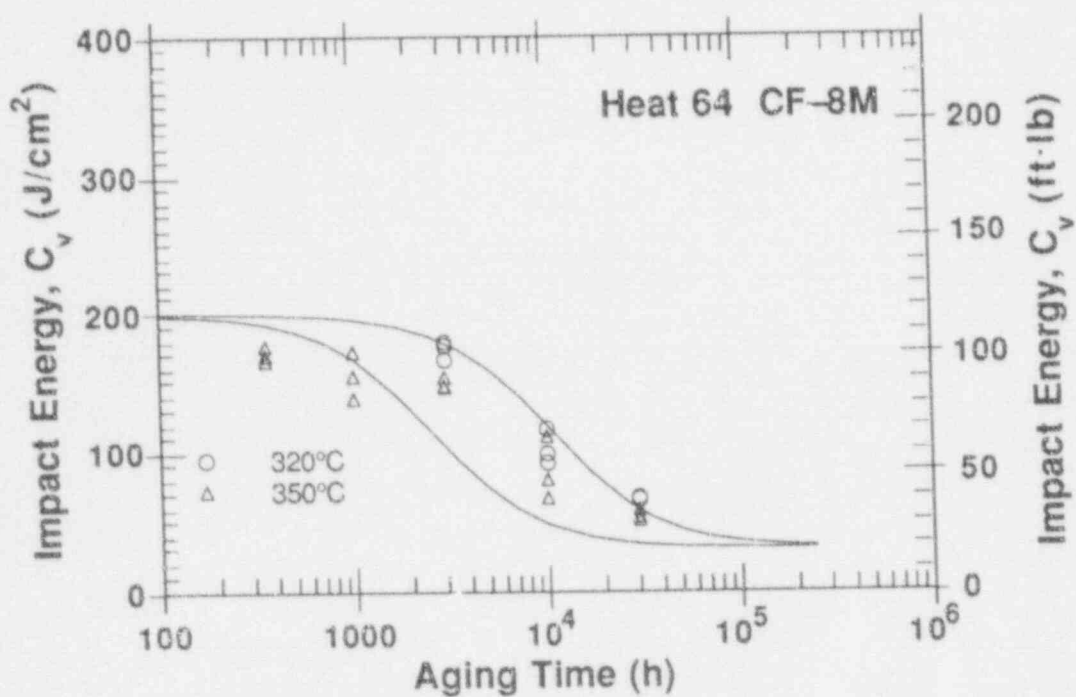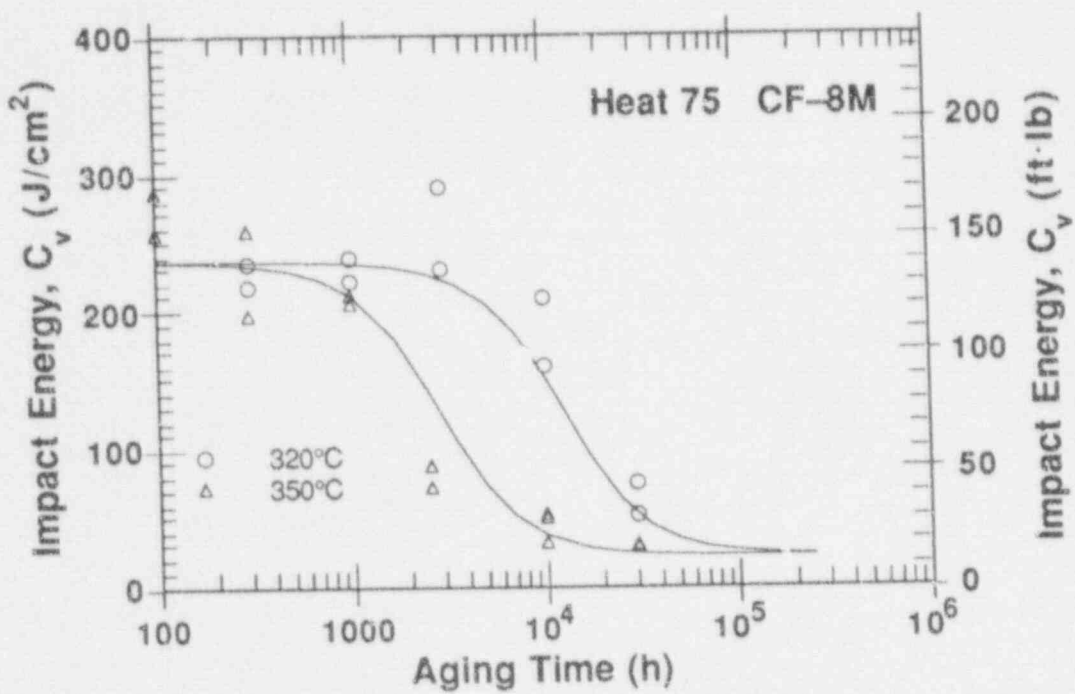
Figure 15. (Contd.)

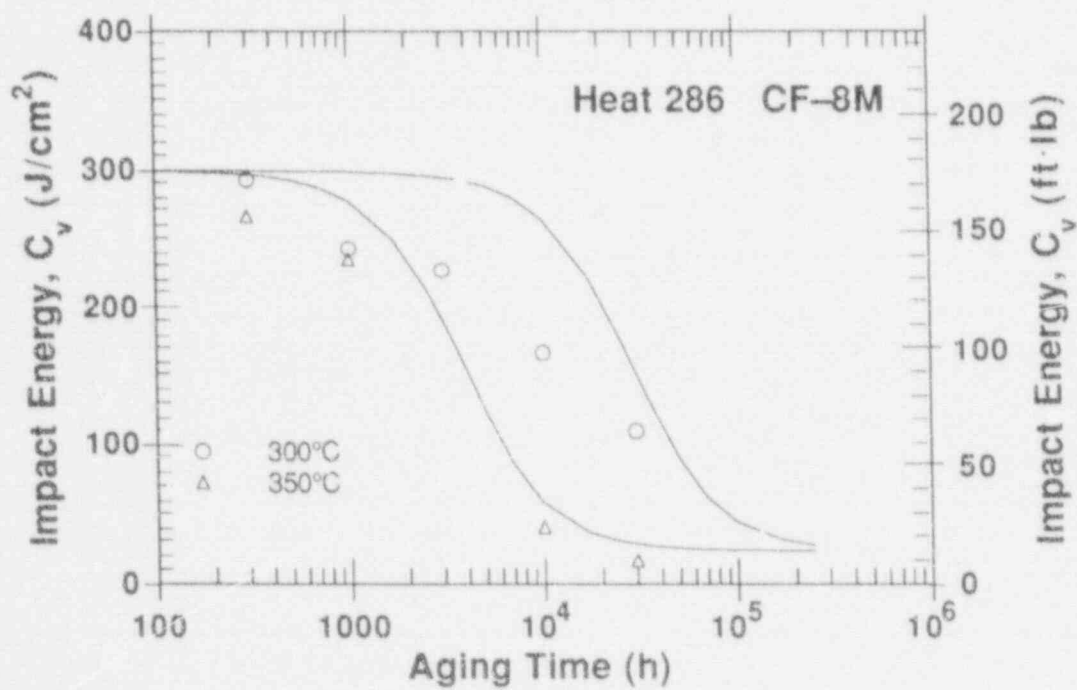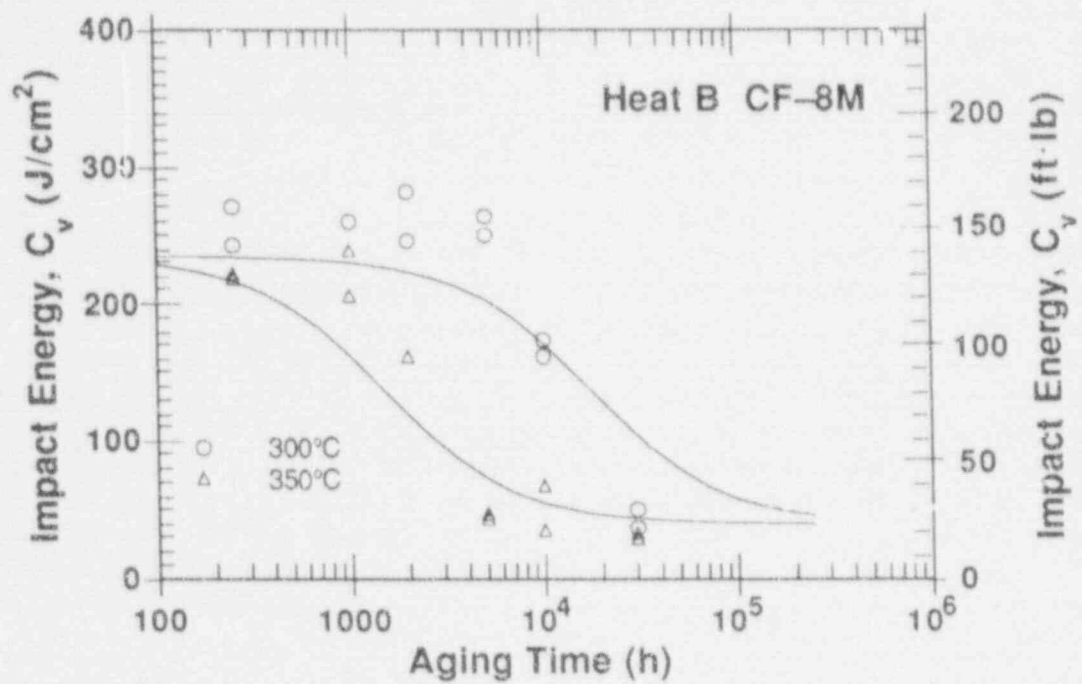Figure 16. *Observed and estimated room-temperature Charpy-impact energy for aged CF-8M cast stainless steel*

Figure 16. (Contd.)

31

behavior at 400°C has a strong effect on the temperature dependence of thermal aging; activation energy for embrittlement is high for heats that show fast kinetics at 400°C and is low for heats with slow kinetics at 400°C. Limited data indicate that the production heat treatment and possibly the casting process influence the aging behavior at 400°C and, therefore, the kinetics of embrittlement. The log of time of aging at 400°C for a 50% reduction in impact energy (constant θ) has been shown to be a useful parameter to characterize the kinetics of thermal embrittlement. θ ranges from 2 to 4 for the various cast stainless steels. A correlation is presented for estimating the activation energy of thermal embrittlement from chemical composition and the aging behavior of the steel at 400°C.

The results also indicate that the kinetics of thermal embrittlement of cast stainless steels is primarily controlled by strengthening of the ferrite matrix. The activation energy for thermal embrittlement determined from measurements of ferrite hardness agree very well with that obtained from Charpy-impact data. Studies on the reembrittlement of recovery-annealed materials indicate that precipitation of G phase has little or no effect on the kinetics of thermal embrittlement. Material parameters that influence the kinetics of embrittlement also effect G-phase precipitation. However, activation energy for thermal embrittlement is generally low for cast stainless steels that contain G phase.

Correlations are presented for estimating the extent and kinetics of thermal embrittlement of cast stainless steels from material information that can be determined from the certified material test record. The extent of embrittlement is characterized by the room-temperature "normalized" Charpy-impact energy. Correlations for the extent of embrittlement at "saturation," i.e., the minimum impact energy that can be achieved for the material after long-term aging, is given in terms of a material parameter that consists of the chemical composition and ferrite morphology. Different correlations are used for estimating the saturation impact energy of CF-3 or CF-8 steels and CF-8M steels. A common expression between material parameter and saturation impact energy is used when metallographic information, i.e., the measured values of ferrite content and mean ferrite spacing, are known. The change in Charpy-impact energy as a function of time and temperature of reactor service is then estimated from the extent of embrittlement at saturation and from the correlation describing the kinetics of embrittlement. Examples for estimating impact strength of cast stainless steel components during reactor service are described.

Acknowledgments

References

1. A. Trautwein and W. Gysel, "Influence of Long Time Aging of CF-8 and CF-8M Cast Steel at Temperatures Between 300 and 500°C on the Impact Toughness and the Structure Properties," in Spectrum, Technische Mitteilungen aus dem+GF+Konzern, No. 5 (May

1981); also in *Stainless Steel Castings*, V. G. Behal and A. S. Melilli, eds., ASTM STP 756, Philadelphia, PA., pp. 165–189 (1982).

2. O. K. Chopra and H. M. Chung, *Long–Term Embrittlement of Cast Duplex Stainless Steels in LWR Systems: Annual Report, October 1983–September 1984*, NUREG/CR-4204, ANL–85-20 (March 1985); *Nucl. Eng. Des.* **89**, 305 (1985).

3. O. K. Chopra and H. M. Chung, *Long–Term Embrittlement of Cast Duplex Stainless Steels in LWR Systems: Annual Report, October 1984–September 1985*, NUREG/CR-4503, ANL–86-3 (January 1986).

4. O. K. Chopra and H. M. Chung, *Long–Term Embrittlement of Cast Duplex Stainless Steels in LWR Systems: Semiannual Report, October 1985–March 1986*, NUREG/CR-4744 Vol. I, No. 1, ANL–86-54 (January 1987).

5. O. K. Chopra and G. Ayrault, in *Materials Science and Technology Division Light–Water-Reactor Safety Research Program: Quarterly Progress Report, October–December 1983*, NUREG/CR-3689 Vol. IV, ANL–83-85 Vol. IV, pp. 129–151 (August 1984).

6. O. K. Chopra and H. M. Chung, in *Materials Science and Technology Division Light–Water-Reactor Safety Materials Engineering Research Programs: Quarterly Progress Report, January–March 1984*, NUREG/CR-3998 Vol. I, ANL–84-60 Vol. I, p. 52 (September 1984).

7. O. K. Chopra and H. M. Chung, "Aging Degradation of Cast Stainless Steels: Effects on Mechanical Properties," in *Environmental Degradation of Materials in Nuclear Power Systems–Water Reactors*, G. J. Theus and J. R. Weeks, eds., The Metallurgical Society, Warrendale, PA., pp. 737–748 (1988).

8. O. K. Chopra and H. M. Chung, "Effect of Low–Temperature Aging on the Mechanical Properties of Cast Stainless Steels," in *Properties of Stainless Steels in Elevated Temperature Service*, M. Prager, ed., MPC Vol. 26, PVP Vol. 132, ASME, New York, pp. 79–105 (1988).

9. O. K. Chopra and H. M. Chung, *Long–Term Embrittlement of Cast Duplex Stainless Steels in LWR Systems: Semiannual Report, April–September 1987*, NUREG/CR-4744 Vol. 2, No. 2, ANL–89/6 (August 1989).

10. O. K. Chopra and H. M. Chung, *Long–Term Embrittlement of Cast Duplex Stainless Steels in LWR Systems: Semiannual Report, October 1987–March 1988*, NUREG/CR-4744 Vol. 3, No. 1, ANL–89/22 (February 1990).

11. O. K. Chopra and H. M. Chung, *Long–Term Embrittlement of Cast Duplex Stainless Steels in LWR Systems: Semiannual Report, April–September 1988*, NUREG/CR-4744 Vol. 3, No. 2, ANL–90/5 (August 1990).

12. O. K. Chopra and A. Sather, "*Initial Assessment of the Mechanisms and Significance of Low–Temperature Embrittlement of Cast Stainless Steels in LWR Systems*," NUREG/CR-5385, ANL–89/17 (August 1990).

13. O. K. Chopra, "Thermal Aging of Cast Stainless Steels: Mechanisms and Predictions," in *Fatigue, Degradation, and Fracture – 1990*, W. H. Bamford, C. Becht, S. Bhandari, J. D. Gilman, L. A. James, and M. Prager, eds., MPC Vol. 30, PVP Vol 195. ASME, New York, pp. 193-214 (1990).

14. O. K. Chopra and H. M. Chung, *Long-Term Embrittlement of Cast Duplex Stainless Steels in LWR Systems: Semiannual Report October 1988–March 1989*, NUREG/CR-4744, Vol. 4, No. 1, ANL-90/44 (May 1991).

15. O. K. Chopra and H. M. Chung, *Long-Term Embrittlement of Cast Duplex Stainless Steels in LWR Systems: Semiannual Report April–September 1989*, NUREG/CR-4744, Vol. 4, No. 2, ANL-90/49 (May 1991).

16. O. K. Chopra, "Estimation of Fracture Toughness of Cast Stainless Steels in LWR Systems," in *Proc. 18th Water Reactor Safety Information Meeting*, U.S. Nuclear Regulatory Commission, NUREG/CP-0114 Vol. 3, p. 195 (April 1991).

17. H. M. Chung and O. K. Chopra, "Kinetics and Mechanism of Thermal Aging Embrittlement of Duplex Stainless Steels," in *Environmental Degradation of Materials in Nuclear Power Systems-Water Reactors*, Proc. 3rd Intl. Symp., G. J. Theus and J. R. Weeks, eds., The Metallurgical Society, Warrendale, PA., pp. 359–370 (1988).

18. H. M. Chung and O. K. Chopra, "Long–Term Aging Embrittlement of Cast Austenitic Stainless Steels – Mechanism and Kinetics," in *Properties of Stainless Steels in Elevated Temperature Service*, M. Prager, ed., MPC Vol. 26, PVP Vol. 132, ASME, New York, 1988, pp. 17–34.

19. H. M. Chung, "Thermal Aging of Decommissioned Reactor Cast Stainless Steel Components and Methodology for Life Prediction," in *Life Assessment and Life Extension of Power Plant Components*, T. V. Narayanan, C. B. Bond, J. Sinnappan, A. E. Meligi, M. Prager, T. R. Mager, J. D. Parker, and K. Means, eds., PVP Vol. 171, ASME, New York, pp. 111–125 (1989).

20. H. M. Chung and T. R. Leax, "Embrittlement of Laboratory and Reactor Aged CF3, CF8, and CF8M Duplex Stainless Steels," *Mater. Sci. and Tech.* **6**, 249-262 (1990).

21. A. L. Hiser, *Tensile and J-R Curve Characterization of Thermally Aged Cast Stainless Steels*, NUREG/CR-5024, MEA-2229, Materials Engineering Associates, Inc. (September 1988).

22. E. I. Landerman and W. H. Bamford, "Fracture Toughness and Fatigue Characteristics of Centrifugally Cast Type 316 Stainless Steel Pipe after Simulated Thermal Service Conditions," in *Ductility and Toughness Considerations in Elevated Temperature Service*, MPC 8, ASME, New York, pp. 99–127 (1978).

23. S. Bonnet, J. Bourgoin, J. Champredonde, D. Guttmann, and M. Guttmann, "Relationship between Evolution of Mechanical Properties of Various Cast Duplex Stainless Steels and Metallurgical and Aging Parameters: An Outline of Current EDF Programmes," *Mater. Sci. and Technol.* **6**, 221-229 (1990).

24. P. H. Pumphrey and K. N. Akhurst, "Aging Kinetics of CF3 Cast Stainless Steel in Temperature Range 300–400°C," *Mater. Sci. and Technol.,* **6**, 211-219 (1990).

25. G. Slama, P. Petrequin, and T. Mager, "Effect of Aging on Mechanical Properties of Austenitic Stainless Steel Castings and Welds," presented at *SMIRT Post–Conference Seminar 6, Assuring Structural Integrity of Steel Reactor Pressure Boundary Components,* August 29–30, 1983, Monterey, CA.

26. Y. Meyzaud, P. Ould, P. Balladon M. Bethmont, and P. Soulat, "Tearing Resistance of Aged Cast Austenitic Stainless Steel," presented at *Intl. Conf. on Thermal Reactor Safety (NUCSAFE 88),* October 1988, Avignon, France.

27. P. McConnell and J. W. Sheckherd, *Fracture Toughness Characterization of Thermally Embrittled Cast Duplex Stainless Steel,* Report NP-5439, September 1987, Electric Power Research Institute, Palo Alto, CA.

28. L. S. Aubrey, P. F. Wieser, W. J. Pollard, and E. A. Schoefer, "Ferrite Measurement and Control in Cast Duplex Stainless Steel," in *Stainless Steel Castings,* V. G. Behal and A. S. Melilli, eds., ASTM STP 756, Philadelphia, PA., pp. 126-164 (1982).

29. J. Sassen, M. G. Hetherington, T. J. Godfrey, G. D. W. Smith, P. H. Pumphrey, and K. N. Akhurst, "Kinetics of Spinodal Reaction in the Ferrite Phase of a Duplex Stainless Steel," in *Properties of Stainless Steels in Elevated Temperature Service,* M. Prager, ed., MPC Vol. 26, PVP Vol. 132, ASME, New York, pp. 65-78 (1988).

30. P. Auger, F. Danoix, A. Menand, S. Bonnet, J. Bourgoin, and M. Guttmann, "Atom Probe and Transmission Electron Microscopy Study of Aging of Cast Duplex Stainless Steels," *Mater. Sci. and Technol.,* **6**, 301-313 (1990).

31. J. E. Brown, A. Cerezo, T. J. Godfrey, M. G. Hetherington, and G. D. W. Smith, "Quantitative Atom Probe Analysis of Spinodal Reaction in Ferrite Phase of Duplex Stainless Steel," *Mater. Sci. and Technol.,* **6**, 293-300 (1990).

32. M. Vrinat, R. Cozar, and Y. Meyzaud, "Precipitated Phases in the Ferrite of Aged Cast Duplex Stainless Steels," *Scripta Met.,* **20**, 1101-1106 (1986).

33. M. K. Miller and J. Bentley, "Characterization of Fine-Scale Microstructures in Aged Primary Coolant Pipe Steels," in *Environmental Degradation of Materials in Nuclear Power Systems-Water Reactors,* Proc. 3rd Intl. Symp., G. J. Theus and J. R. Weeks, eds., The Metallurgical Society, Warrendale, PA., pp. 341-349 (1988).

34. T. Magnin and F. Moret, "Mechanical Twinning in Ferritic Stainless Steels," *Scripta Met.,* **16**, 1225-1228 (1982).

35. T. Magnin, J. LeCoze, and A. Desestret, "Twinning and Stress Corrosion Cracking of Ferritic Phase of Duplex Stainless Steels," in *Duplex Stainless Steels,* R. A. Lula, ed., American Society for Metals, Metals Park, Ohio, pp. 535-551 (1983).

36. M. Anglada., M. Nasarre, and J. A. Planell, "High Temperature Mechanical Twinning of Two Fe–Cr–Mo–Ni Ferritic Stainless Steels," *Scripta Met.*, **21**, 931–936 (1987).

37. O. K. Chopra, "Studies of Aged Cast Stainless Steel from the Shippingport Reactor," in *Proc. 18th Water Reactor Safety Information Meeting*, U.S. Nuclear Regulatory Commission, NUREG/CP–0114 Vol. 3, p. 369 (April 1991).

P. H. Pumphrey, National Power, Technology and Environment Center, Leatherhead, Surrey, UK

V. N. Shah, EG&G Idaho, Inc., Idaho Falls

V. K. Sikka, Oak Ridge National Laboratory

A. Singh, Unical Science & Technology Division, Brea, CA

G. Slama, Framatome, Paris La Defense, France

G. D. W. Smith, Oxford University, Oxford, UK

H. D. Solomon, General Electric Co., Schenectady, NY

D. M. Stevens, Lynchburg Research Center, Babcock & Wilcox Co., Lynchburg, VA

L. Taylor, Nuclear Electric plc., Chelsford Rd., Knutsford, Cheshire, UK

J. M. Vitek, Oak Ridge National Laboratory

J. Wilks, AMOCO, P. O. Box 3011, Naperville, IL

2. TITLE AND SUBTITLE

Long-Term Embrittlement of Cast Duplex Stainless Steels in LWR Systems

Semiannual Report
October 1989-March 1990

3. DATE REPORT PUBLISHED

MONTH	YEAR
July	1991

4. FIN OR GRANT NUMBER

A2243

5. AUTHOR(S)

O. K. Chopra, L. Y. Bush

6. TYPE OF REPORT

Technical; Semiannual

7. PERIOD COVERED *(Inclusive Dates)*

October 1989-March 1990

10. SUPPLEMENTARY NOTES

11. ABSTRACT (200 words or less)

This progress report summarizes work performed by ANL on long-term thermal embrittlement of cast duplex stainless steels in LWR systems during the six months from October 1989 to March 1990. The results from Charpy-impact tests and microhardness measurements of the ferrite phase for several heats of cast stainless steel aged up to 30,000 h at 290–400°C are analyzed to establish the kinetics of thermal embrittlement. Correlations are presented for predicting the extent and kinetics of thermal embrittlement of cast stainless steels from material information that can be determined from the certified material test record. The extent of embrittlement is characterized by the room-temperature "normalized" Charpy-impact energy. Based on the information available, two methods are presented for estimating the extent of embrittlement at "saturation," i.e., the minimum impact energy that would be achieved for the material after long-term aging. The first method utilizes only the chemical composition of the steel. The second method is used when metallographic information on the ferrite morphology, i.e., ferrite content and mean ferrite spacing of the steel, is also available. The change in Charpy-impact energy as a function of time and temperature of reactor service is then estimated from the extent of embrittlement at saturation and from the correlations describing the kinetics of embrittlement, which is expressed in terms of the chemical composition and aging behavior of the steel at 400°C.

12. KEY WORDS/DESCRIPTORS *(List words or phrases that will assist researchers in locating this report.)*

Cast duplex stainless steel
Thermal aging
Embrittlement
Microhardness
Impact strength

13. AVAILABILITY STATEMENT

Unlimited

14. SECURITY CLASSIFICATION

(This Page)

Unclassified

(This Report)

Unclassified

15. NUMBER OF PAGES

16. PRICE

UNITED STATES
NUCLEAR REGULATORY COMMISSION
WASHINGTON, D.C. 20555

———

OFFICIAL BUSINESS
PENALTY FOR PRIVATE USE, $300